Determination of Structural Health of the Lincoln Parking Deck at YSU

by

Meera Elizabeth Maxy

Submitted in Partial Fulfillment of the Requirements

for the Degree of

M.S. in Civil Engineering

in the

Civil and Environmental Engineering

Program

YOUNGSTOWN STATE UNIVERSITY

May, 2018

Determination of Structural Health of the Lincoln Parking Deck at YSU

Meera Elizabeth Maxy

I hereby release this thesis to the public. I understand that this thesis will be made available from the OhioLINK ETD Center and the Maag Library Circulation Desk for public access. I also authorize the University or other individuals to make copies of this thesis as needed for scholarly research.

Signature:

_____

Meera Elizabeth Maxy, Student Date

Approvals:

_____

Dr. AKM Anwarul Islam, P.E., Thesis Advisor Date

_____

Dr. Richard A. Deschenes, Committee Member Date

_____

Dr. Jai K. Jung, Committee Member Date

_____

Dr. Salvatore A. Sanders, Dean of Graduate Studies Date

ABSTRACT

The Lincoln Parking Deck at Youngstown State University has been serving as one of the most important structures on campus since the 1970s. It is a multi-level parking deck consisting of two entries and exit points from Lincoln Ave and Arlington St. Due to aggressive environmental conditions in Northeast Ohio, this structure has undergone deterioration, which ranges from mild in some places to extreme in certain locations. This research delves into the potential decrease in safety of the structure due to corrosion in reinforcement and other structural damages. Even after undergoing routine maintenance checks, the structure shows signs of corrosion within the embedded concrete, which are now visible from the outside. This research mainly focuses on detecting the causes of corrosion in reinforcement and suggesting remediation to overcome corrosion in both new and existing structures. Use of advanced non-destructive techniques, such as Ground Penetrating Radar and the Profoscope, has revealed crucial details that could help understand corrosion in various structures. Visual inspection also led to the discovery of corrosion on the deck which was not mentioned in the renovations. The data obtained from the structural drawings were incorporated into probabilistic equations to determine the present condition of the parking deck using corrosion modelling. A structural analysis was performed on the parking deck to evaluate the strength of the materials and the results obtained were found to be satisfactory. The results indicate the parking garage to be structurally adequate at the time of the experiments. Based on the findings, appropriate remedial measures were suggested to avoid further corrosion.

Detecting corrosion and undertaking proper rehabilitation would help YSU on maintenance. It may also help commuters use the parking deck with ease and comfort. A

considerable number of students and staff use the Lincoln Parking Deck daily. If the corrosion becomes severe, then the structure might have to be closed. Any inspection, maintenance, or replacement will require temporary closing of the parking deck, which is not very expected with such an extensive daily use of the deck.

ACKNOWLEDGEMENTS

First and foremost, I would like to express my deepest gratitude to Dr. AKM Anwarul Islam, P.E., my thesis advisor for his expert advice and encouragement throughout this research. This research would not have been possible without his continued support and inspiration. I would also like to thank him for his abundant patience and time in helping me achieve the desired results in this research. I take this opportunity to extend my sincere gratitude to my thesis committee members, Dr. Richard A. Deschenes and Dr. Jai. K Jung for their valuable time and suggestions.

I would also like to take this opportunity to thank the Facilities Maintenance Services (FMS) at YSU for providing the structural drawings of the Lincoln Parking Deck for my research, the technical team from Geophysical Survey Systems, Nashua for assisting me with the GSSI SIR-4000 and RADAN, Department of Civil and Environmental Engineering to have given me this opportunity to be a part of the Civil Engineering community here at YSU, our department secretary Ms. Linda Adovasio for helping me with my daily activities at the department, Dr. Holly Martin from the Chemical Engineering department for helping me with the chemical tests, my counselor, Ms. Anne Lally for molding me into a better person both physically and emotionally, my friend and colleague, Romit Thapa for helping me record the images of the corrosion locations on the parking deck.

This research would have been impossible without my best friend, Vijay Kumar whom I adore and has been everything to me. Thank you for taking your time off from your busy

schedule to help me debug the MATLAB codes. Also, thank you for being a part of my life, I love you!

I would also like to thank my best friends, Hridyesh Mangalath, Apuroop Naidu and Soumya B.K., who are more like my family for their endless love and support throughout this research. You guys were always there whenever I needed you the most. I appreciate all your help and time.

I would also like to extend my sincere gratitude to my other friends and colleagues, especially Dr. Matt Caputo, Tom Gabriel, Nikhil Chougule, Hari Dhungel, Ekaraj Ghimire and Richard Yovichin for all their love and constant motivation throughout this period.

Last but not the least, I thank God for giving me such a wonderful and supportive family. Words are not enough to thank them for what they have all done for me, especially my parents Sheena Maxy, Maxy Sebastian and my brother Abhishek Maxy who were always there to support me emotionally during this journey, without whom this feat could not have been accomplished. I am grateful to each one of you. I love you all loads!

TABLE OF CONTENTS

LIST OF FIGURES

LIST OF TABLES

NOMENCLATURE

$E°_A$ = standard electrode potential of steel at anode ($E°_A$= -0.44 V)

R_c = gas constant (R_c = 8:314 J/°K)

F = Faraday's constant (96,487 Coulomb per mole of electrons or Ampere-second)

T = absolute temperature (298.15 K)

n = total number of electrons taking part in the reaction (*n*=2)

[Fe] = activity of Fe molecule in steel bar (1)

i_{corr} = corrosion current density (A/m^2)

C_t = total chloride content (kg/m^3 of concrete)

T = average temperature of the year (K)

R_C = Ohmic resistance of the cover concrete (Ω)

t = time-period after corrosion initiation (years)

x_{corr} = average corrosion rate in the radial direction (μm/year)

t = time-period (years)

X_{corr} = total amount of corroded steel in radial direction (m)

R_{corr} = parameter for the type of corrosion (carbonation = 1; chlorination = 5.5)

$X_{corr,cr}$ = depth of corroded steel at the time of cracking (m)

a_1 = $7.44e^{-5}$ (m)

a_2 = $7.30e^{-6}$ (m)

a_3 = -1.74^{e-5} (m/MPa)

C = concrete clear cover (m)

d_{ini} = initial bar diameter (m)

$f_{t,ch}$ = characteristic splitting tensile strength of concrete (MPa)

b = parameter for the position of the bar (top reinforcement = 8.6 μm/μm, bottom reinforcement = 10.4 μm/μm)

W^d = critical crack width for spalling (characteristic value 0.001 m)

W_0 = width of initial crack (m)

$X_{corr,sp}$ = depth of corroded steel at the time of spalling (m)

Chapter 1. Introduction

1.1 Problem Statement

The recent advancement in engineering and technology has set the stage for innovation in determining structural health of existing infrastructure (Koch et al., 20002; Bertolini et al., 2013). Yet the biggest challenge in preserving the structural health of a concrete structure is corrosion in reinforcement (Berkowskia et al., 2013). Corrosion acts as the primary concern in civil engineering industry as it disrupts the health and integrity of a structure. Each structure is built with a minimum investment to last its intended life; however, corrosion disrupts the purpose by compromising its structural health. This research aims at finding the structural health of 'Lincoln Parking Deck' on the campus of YSU in Youngstown, Ohio.

The Lincoln Parking Deck is a landmark structure on campus that has undergone severe corrosion at various locations. The construction of this structure began in 1971. It is a three-level parking deck with optional parking on the roof. According to the available structural drawings and related repair information, it was determined that the first renovations were done in 1985, and the latest set of repairs was performed in 2012. According to the past research, the typical life of a reinforced concrete structure is between 50 and 100 years (Berkowskia et al., 2013). This parking deck is roughly 45 years old.

Concrete with reinforcing steel plays a vital role in producing durable reinforced concrete structures. There are numerous technologies that have helped improve the properties of these materials. Reinforced concrete structures are always subjected to various

deterioration activities that impact their strength and intended purpose. Corrosion in reinforcement is the most common phenomenon observed in reinforced concrete structures while premature corrosion is unexpected (Berkowskia et al., 2013). Based on the studies conducted by Vaysburd and Emmons (2000), premature corrosion occurs due to three primary reasons, such as cracking of components due to excessive drying, electrochemical discrepancies between the concrete surface and the steel reinforcement, and finally, the alterations caused due to the existing repairs within the structure.

1.2 Research Objectives

The main objectives of this research were to determine the causes of corrosion in the Lincoln Parking Deck and to check its structural integrity and health, and to suggest some possible remedial measures. This research concentrates on the effects and mechanisms of chlorination and carbonation on the parking deck as these together forms an appropriate environment for corrosion initiation. With the help of advanced geophysical techniques, such as a GSSI SIR 4000 bridge scanner and a Profoscope, the size, location and spacing of reinforcement on the corroded locations in the parking deck were determined. These details were necessary to help in the evaluation of corrosion formation over the years. Using probabilistic equations, deterioration models were also analyzed to understand the effects of chlorination and carbonation during the propagation phase of corrosion. These models depict the rate at which corrosion has progressed since the inception of the structure.

Chapter 2. Literature Reviews

2.1 Background

The history of parking structures dates to the 1900s. The need for transportation increased with the increase in population. According to the National Building Museum, there were about 23 million cars on the streets of the United States by 1930s. As cars filled up the streets, finding a parking spot became tougher day by day. The solution to this problem was given by the construction of parking structures across several major cities in the United States (Melsen, 2012).

The first of many parking structures were constructed mainly as single level units. The pioneer in multi-level parking structures is the five-star hotel called La Salle in Chicago, Illinois. Its parking decks were designed in 1918 by the architectural firm, Holabird and Roche. In order to utilize the maximum space for the increasing number of cars, split-level floors for parking were introduced. The first such structure was known as D'Hump ramp system (Kansas Public Radio, 2009).

Parking structures are relatively complex structures in the field of structural design and construction (Berkowskia et al., 2013). According to ACI, a parking structure with at least 40% opening is called an 'open parking structure' (ACI 330R, 2001). The Lincoln Parking Deck, as shown in Fig. 2-1, falls under this category as more than 40% of the entire structure is unenclosed.

An open parking deck is considered as a bridge since much of the structure is open to the outer environment and each deck resembles a bridge deck. Each floor is designed to carry a lateral bumper load at the barrier walls as well. The top floor or roof of a typical multi-level parking deck generally carries a combination of snow and rain loads along with the

typical dead and live loads from parked or moving vehicles. In most cases, natural threats caused due to precipitation, solar heating, and radiation from ultra-violet and infra-red rays attack the top levels, while compared to the rest of the levels in the structure (ACI 362.1R, 1997).

Figure 2-1: A perspective view of the Lincoln Parking Deck from Lincoln Ave.

The run-off water from rain or snow must be properly guided to the sewage outlets to avoid standing water, especially during the winter months. The standing water contains deicing salts carried by the vehicles and seeps into the concrete. Other factors leading to parking deck's loss of strength would be spalling of concrete due to repeated loadings on the deteriorated areas, freeze-thaw cycles and salt scaling (ACI 362.1R, 1997).

Rapid changes in temperature cause expansion and contraction, which initiates crack in the structural components, such as slabs, beams and columns. These cracks increase

ingress of chloride ions that are ultimately responsible for corrosion in the structure. On the other hand, a closed parking structure must overcome the pressure differences caused from wind and other elements, which counteract the internal pressure caused within the structure (ACI 362.1R, 1997).

The structures have been classified into five different zones based on the permeability of concrete, moisture content prior to freezing (no deicing salts are used) and concrete exposed to deicing, brackish water or sea water. ACI 318 (2002) classifies the five exposure zones as shown in Fig. 2-2 based on the temporal conditions (ACI 362.1R, 1997);

Figure 2-2: Exposure Zones in the United States (ACI 362.1R, 1997).

i. Zone I - These are those areas where freezing rarely occurs. The use of deicing salt is limited and is not considered in these cases. The area which lies

to the south of Zone II and to the west of Zone III with an exception to areas above an elevation of 3,000 ft are classified as Zone I.

ii. Zone II - The areas which lies to the south of Zone III, encloses an area of about 100 miles from the south of the Interstate Highway 40 to the Atlantic Ocean west located in the Continental Divide. This also includes all the areas under Zone I, which are present between an elevation of 3,000 ft and 5,000 ft. The areas include the State of Oregon and Washington west of the Cascade ranges excluding the areas above the elevation of 5,000 ft. Freezing occur quite rarely and the use of deicing salt is little to zero in Zone II.

iii. Zone III - Zone III comprises of the areas to the north and within 100 miles south of Interstate Highway 70, extending from the west of the Atlantic Ocean to Interstate Highway 15, north to the Interstate Highway 84, northwest to Portland Oregon, west to the Pacific Ocean including areas under Zone I and II above the elevation of 5,000 ft. Deicing salts are commonly used in Zone III since freezing is a common problem.

iv. Coastal Chloride Zone I (Zone CC-I) - This constitutes the areas of Zone I and within 5 miles of the Atlantic Ocean, Gulf of Mexico, Pacific Ocean and the Great Salt Lake.

v. Coastal Chloride Zone II (Zone CC-II) - This constitutes the areas, which are in Zones I and II, and at a distance within one-half mile of the salt water bodies mentioned in Zone CC-I.

Routine maintenance plays a significant role in helping the structure maintain its desired strength. The maintenance checks aid in understanding the gradually deteriorating

condition of the structure. They also help in undertaking precautionary measures in order to avoid any future corrosion that threatens the strength and integrity of a reinforced parking deck. Many reinforced structures are subjected to various adversities such as loss of reinforcement area due to corrosion, delamination and spalling that could compromise the structure's strength and serviceability to half of its expected design life. This scenario could be averted with the use of suitable restoration measures (Vaysburd and Emmons, 2000).

Issues identified with the durability of reinforced concrete include structural design and execution, satisfactory insurance of constructional components against various ecological impacts, problems related to the appraisal of the structural condition after an accident, and on-time repair and maintenance of structures (Berkowskia et al., 2013).

The major cause of structural deterioration is corrosion of steel reinforcement. Corrosion affects the life expectancy, stability and aesthetics of a structure. Corrosion is a natural process caused due to the chemical reactions between concrete, reinforcing steel and the environment. According to studies funded by the Federal Highway Administration and NACE International, CC Technologies Laboratory conducted a survey which suggested the annual costs for structural rehabilitation due to corrosion in structures in the U.S. and Canada between 1999 and 2001 was roughly around $276 billion and $74 billion respectively. About 35% of this cost could be avoided if proper maintenance has been provided to eliminate or to detect corrosion at an earlier stage (Koch et al., 2002).

The article written by Taylor (1997) discusses deterioration of various concrete structures, such as bridges, marine structures, tunnels, parking garages and railway sleepers. This has initiated engineers to perform research on the micro-properties of

concrete. He also added that in the present setting of global development and the changing demeanor in public on environmental issues, toughness of concrete as an engineering material in the world of construction and development needs to be reviewed and re-evaluated (Taylor, 1997).

Berkowskia et al., (2013) has illustrated the state of a structure during its time of service. Their study proposed a 'performance indicator' that varies with time. Initially, the capacity of a structure is found to be steady. However, after a certain period, the capacity decreases. The reason for this could be due to the material corrosion or cracking in reinforced concrete structures. At this point, the structure reaches its maximum Serviceability Limit State (SLS). On the other hand, if there are no appropriate measures taken to stop the structural deterioration then the structure's condition is said to intensify to achieve its Ultimate Limit State (ULS). If repairs are performed on time, then the structure's service life can be extended (Berkowskia et al., 2013).

2.1. Corrosion

Concrete is the most widely used building material in the world. It consists of a mixture of cement, sand, aggregates and water. The durability of concrete is an important aspect when serviceability and stability of the structure are considered. Once the concrete achieves its maximum strength, the voids within the mortar attracts chemicals from the surface (Hansson et al., 2012). Most of the penetration of chlorides happens because of the pressure and ionic differences between surface water and the concrete pore structure (Hájková, 2015). The combination of both steel and concrete helps the structure in attaining the necessary durability.

Corrosion is an electrochemical process that affects the durability of structural members. It is a combination of reactions, such as oxidation and reduction which attacks the steel members, there-by deteriorating the integrity of the structure. When steel undergoes corrosion, a large amount of the material converts into rust resulting in the loss of reinforcement. Since the volume of rust is larger than the original volume of steel, this additional volume expands into the surrounding concrete eventually causing cracking, delamination and spalling (PCA, 2002).

The primary element of steel is iron which is derived from iron ore. During the manufacturing process, a large amount of energy is added to the conversion of iron ore into steel. Steel tends to the natural state; iron oxide or simply rust (PCA, 2002). According to Portland Cement Association (PCA, 2002), corrosion takes place in the presence of these four components: minimum of two metals at different energy levels, an electrolyte and a metallic connection. The electrons and ions present within the metal flow freely. In concrete, the reinforcing bar acts as the anode and the concrete acts as the electrolyte. During the electrochemical process (oxidation), the anode loses its electrons which travel to the nearby concrete. This reaction produces ferrous ions. This process is described by Eq. 2.1 and is called 'half-cell oxidation' or 'anodic reaction' (PCA, 2002).

$$2Fe \rightarrow 2Fe^{2+} + 4e^{-} \tag{2.1}$$

These free electrons flow towards the cathode. Here, these electrons combine with pore water and oxygen present within the concrete and forms hydroxyl ions through the reaction known as 'reduction' as shown in Eq. 2.2 (PCA, 2002).

$$2H_2O + O_2 + 4e^{-} \rightarrow 4OH^{-} \tag{2.2}$$

In order to sustain the electrical equilibrium present within the specimen, Eq. 2.3 shows that the ferrous ions react with the hydroxyl ions to form iron oxides, also known as rust (PCA, 2002).

$$2Fe^{2+} + 4OH^{-} \rightarrow 2Fe\,(OH)_2 \qquad (2.3)$$

These hydroxides further tend to react with the surrounding oxygen and form much higher oxide states. This increases the area of corrosion as they react with the dissolved oxygen. As the area of corrosion increases, the internal stresses begin to develop gradually causing cracking, delamination and spalling of the concrete, as shown in Fig. 2-3. At this point, the steel naturally remains in a passive state within the concrete (Ann and Song, 2007).

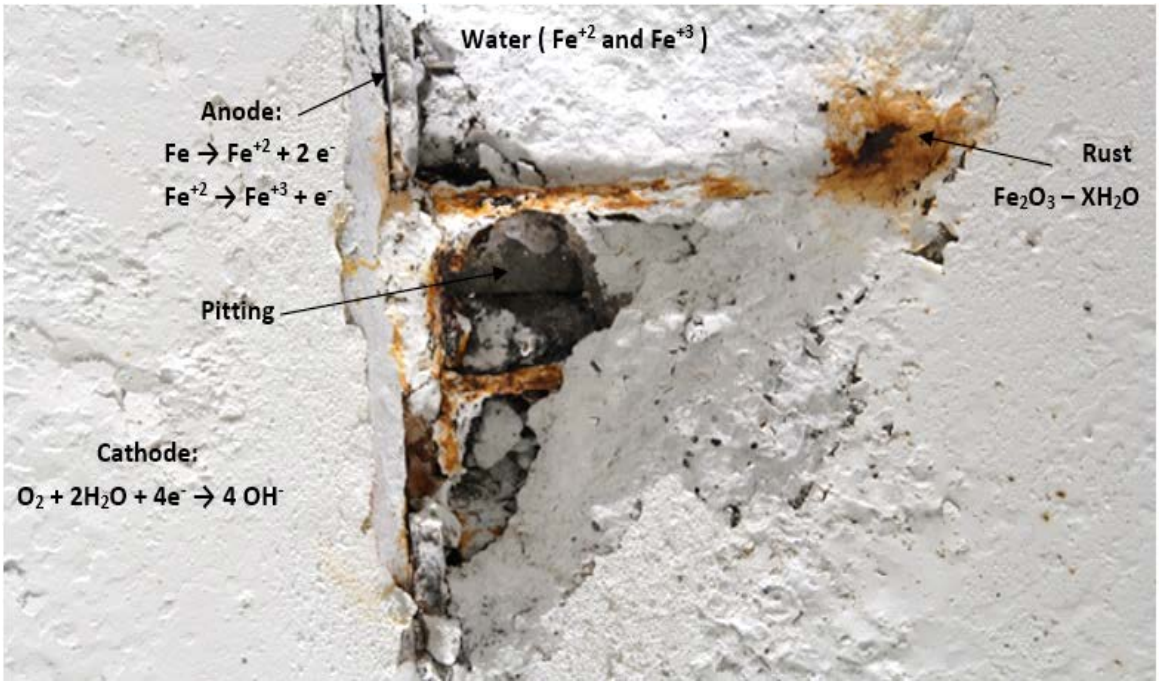

Figure 2-3: Formation of corrosion at the bottom of the parking deck.

Due to the high pH of pore solution in the concrete, the rate of corrosion is relatively less. A protective layer is formed when the steel remains in a passive state. The chemical composition of this layer is controlled by oxides, hydroxides or oxy-hydroxides formed with the help of pH and the electric potential. The passive layer becomes unstable if the pH value decreases below 9 due to chloride ions in solution (Hansson et al., 2012).

2.2. Corrosion Cell

Corrosion is an electrochemical process. The mechanism of current passing through the corroded steel is similar to that of a battery, and thus corrosion can be analyzed in an analogous manner. The corrosion in reinforcement is initiated due to the coupled reactions of both anode and cathode at the presence of the concrete pore water, which acts as a complex electrolyte. Reactions at anodes and cathodes are collectively called as half-cell reactions (Ahmad, 2003).

Oxidation is an anodic reaction and the reduction of oxygen is the cathodic reaction. These electrochemical reactions strongly influence the corrosion rate in reinforcing steel. The Nernst equation used in the studies by Ahmad (2003), gives the expression for the anodic potential in the anodic reaction, as shown by Eq. 2.4. Equation 2.4 was further converted in terms of $[Fe^{2+}]$ to make it a simpler expression as demonstrated by Eq. 2.5.

$$E_A = E°_A + (R_C T / nF) \ln ([Fe^{2+}]/ [Fe]) \quad (2.4)$$

$$E_A = -0.44+0.0296 \log[Fe^{2+}] \text{ (in V)} \quad (2.5)$$

The Nernst equation also gives the expression for the cathodic potential in the cathodic reaction shown in Eq. 2.6. This equation can be modified in terms of $[O_2]$ and pH.

$$E_C = E°_C + (R_C T / nF) \ln [O_2] [H_2O]^2/ [OH^-]^4 \quad (2.6)$$

From the equations obtained to calculate the potentials from the anode and cathode, the electromotive force (e) in corrosion cell can be determined by Eq. 2.7. The electromotive force is obtained from the potential differences between the anode and the cathode, as shown in Eq. 2.8.

$$e = E_C - E_A \tag{2.7}$$

$$e = 1.229 + 0.0148 \log [O_2] - 0.0591\, pH + 0.44 - 0.0296 \log [Fe^{2+}] \tag{2.8}$$

2.3. Types of Corrosion

Much of the research conducted by the Corrosion Technology Laboratory at Kennedy Space Center, NASA, and other researchers have identified and classified different types of corrosion depending on the activities on the surface of the metal and its surroundings. They are explained as follows.

2.3.1. Pitting corrosion

Chloride ions, which are present within the metal, combine with oxygen and act as a depolarizer to form oxygen salts. This helps in the formation of pits on the surface leading to corrosion. Acidic environments with low pH also contribute in the formation of rust. Pitting corrosion poses much more threats than other types of corrosion since the formation of rust happens gradually over time without any immediate signs of warning (Hájková et al., 2015). This research mainly focuses on pitting corrosion as that was the most common type of corrosion observed in the Lincoln Parking Deck.

2.3.2. Uniform corrosion

Uniform corrosion usually takes place with the help of chemical agents, such as acids, causing a direct chemical attack on the structure, as shown in Fig. 2-4. From observations, this could be identified as a dulling of the surface of the metal embedded within the concrete. This is also called as localized or general corrosion. This could become a major maintenance issue if proper care is not provided before corrosion becomes critical. The application of chemical-resistant protective coatings could be a possible solution for such corrosions (Farny and Kosmatka, 1997).

Figure 2-4: Uniform corrosion on the pipes in the Lincoln Parking Deck.

2.3.3. Dissimilar metal corrosion

Each metal has a distinct electrochemical potential because of different chemical composition. When two dissimilar metals, such as steel and aluminum, come in contact with each other, it leads to corrosion (Hansson et al., 2012). This type of corrosion is seen in places when the embedded aluminum railings come in contact with reinforcing steel

(PCA, 2002). Figure 2-5 shows corrosion formed due to two dissimilar metals since the angles were made of ASTM A-36 steel and the bolts were made from carbon steel.

Figure 2-5: Dissimilar corrosion between deck metal plates and bolts in the Lincoln Parking Deck.

2.3.4. Galvanic corrosion

Galvanic corrosion is also an electrochemical process. It occurs when two dissimilar metals come in contact in the presence of an electrolyte and a conductive path. It is similar to dissimilar corrosion and is usually seen at the metal joints. Magnesium is the most active metal while Platinum is the least active in terms of electric potential. Thus, most of the galvanic corrosion happens between magnesium and aluminum. The addition of metals such as magnesium, tin and lead in concrete leads to alkaline reactions leading to cracking (Hansson and Poursaee, 2012).

2.3.5. Microbial corrosion

Microbial corrosion is also called Microbiologically Influenced Corrosion. It is caused by the active presence of microbes. The biofilm is produced when the surface is exposed to

air, or the presence of stagnant water around the structural element occurs. This biofilm acts as a protective layer thus accelerating the formation of corrosion and its by-products. The main purpose of the biofilm is to accumulate the corrosive chemicals towards the production of biofilm in that particular area which is considered as extremely aggressive in nature when compared to near-by areas. The use of biocides can help prevent microbial corrosion (Kobrin, 1993).

2.4. Causes of Corrosion

Some of the major causes of corrosion are discussed below.

2.4.1. Availability of oxygen and moisture

Both, available oxygen and moisture may initiate corrosion by achieving the required electrochemical reactions of the corrosion cell. Oxygen and moisture together help in the production of more hydroxyl ions, which in turn help in the formation of $Fe(OH)_2$, also known as rust. Without the presence of enough oxygen, cathodic polarization or reduction reaction does not occur. This shows that oxygen acts as a major component in the formation of corrosion (Ahmad, 2003).

2.4.2. Relative humidity and temperature

The relative humidity also has major influence on the carbonation of concrete. The rate of corrosion is directly proportional to the increase in temperature and relative humidity. As the relative humidity increases within the prescribed limits such as 50% to 70%, the rate of carbonation decreases. A rise in temperature values increases the electrode reaction rate and enhances corrosion (Cahyadi et al., 1993).

2.4.3. Rate of carbonation of concrete

Calcium hydroxide in hydrated cement reacts with carbon dioxide causing the concrete to become acidic. Carbonation reduces the pH of concrete leading to loss of passive film from the embedded reinforcement. This leads to the exposure of the reinforcing steel to the corrosive environment. Corrosion takes place when the pH value drops below 12. At a higher pH, a passivating layer is formed around the reinforcing steel. As the carbonation tends to be acidic in pore solution, at a pH of 8.0 or below, this passive film from the steel starts corroding. As the pH drops below 7, extensive corrosion takes place leading to structural deterioration (Šavija and Lukovic, 2016).

2.4.4. Water-cement ratio

Water-cement ratio impacts the strength, durability and permeability of concrete. The permeability of concrete influences the corrosion rate. The chloride ingress depth increases with an increase in the water-cement ratio (ACI 330R, 2001).

2.4.5. The Extensive use of supplementary cementitious materials

Supplementary Cementing Materials are imperative to improving the corrosion protection provided for the structures. This could be in the form of fly ash, slag cement, natural pozzolans or silica fume. Supplementary Cementing Materials (SCM) with a low water-cement ratio reduces the corrosion potential, decreasing the need for corrosion protection. Experiments must be conducted to determine the amount of SCM to be used in concrete. This is necessary to determine the maximum amount of chloride ion present in the SCM. If the materials are found to be incompatible due to excess chloride ion content, it leads

to rapid slump loss. This increases the demand for water reduces the resistance to corrosion on reinforced concrete (ACI 222.3R, 2011).

2.4.6. Curing conditions of concrete

Curing helps in attaining the desired characteristics of concrete such as strength, elastic modulus and freezing-and-thawing resistance. It also helps in developing high electrical resistivity. Curing also helps the concrete become impermeable to water content to a limited extent. This indeed helps in minimizing the pores present in the concrete thereby decreasing porosity. In one of the studies conducted by Hansson and Sorensen (1990) it is shown that through proper curing of concrete the reinforcing steel gains internal resistance against corrosion of steel (ACI 222.3R, 2011; Hansson and Sorensen, 1990).

2.4.7. Consolidation of concrete

Concrete should achieve adequate consolidation with the lowest feasible water-cement ratio as possible. After conducting various tests, researchers have identified the effects of the degree of consolidation and water-cement ratio on the amount of chloride ion ingress into concrete. After several observations, concrete with a water-cement ratio of 0.40 resisted the ingress of chloride ions as compared to concrete with water-cement ratios of 0.50 and 0.60 (ACI 309R, 2005). It was also seen that concrete with poor consolidation and a water-cement ratio of 0.32 permitted the ingress of chloride-ions into the concrete. Researchers have conducted experiments by applying salt on the concrete on an everyday basis before the chloride content reached its critical value of 0.20 in acid-soluble testing. Upon analyzing the samples, it was suggested that a thickness of 40 mm (1.5 in) and a water-cement ratio of 0.40 would be sufficient to protect the reinforcing steel embedded

in the concrete from corrosion for approximately 800 salt applications (Daczko and Attiogbe, 2003; ACI 309R, 2005).

Chapter 3. Evaluation of Lincoln Parking Deck

3.1. Overview

As per ACI 362.1R (1997), the use of deicing salt is prohibited in parking deck, but this does not completely prevent the intrusion of deicing salts into the deck. The most common method of ice control on roads and highways is deicing salt. The chloride ions (Cl^-) present in the deicing salt attack the rebar and causes chlorination-induced corrosion. Even though the Facilities Maintenance Services (FMS) Department at YSU does not use deicing salt on the parking deck, the vehicles that enter the deck carry some amount of deicing salt from the streets. The vulnerability of reinforced concrete structures to chloride ions contributes to corrosion and the formation of rust.

Some economical solutions to the widespread problem of corrosion will safe-guard the parking deck from further deterioration. Studies have shown various methods of preventing corrosion in reinforced concrete structures (Dallin et al., 2015; Ahmed et al., 2017), which are discussed in Chapter 5.

3.2. Causes of Deterioration

The construction of a parking deck involves major design considerations that are similar to that of bridge design. Both are large open structures when compared to a typical concrete building. The construction is carried out differently in places with warm and humid climates compared to the ones where the winter is severe. In fact, places where it snows regularly during winter have a high probability of corrosion because of the extensive use of deicing chemical agents (ACI 222.3R, 2011).

The main causes for corrosion in Lincoln Parking Deck are explained below. The combination of several types of corrosion could have influenced in the development and progression of corrosion in the structure. A detailed review of these causes would help in identifying the possible remedies for the deterioration of the Lincoln Parking Deck.

3.2.1. Deicing salt

The chemical agents in deicing salts instigate the formation of corrosion in reinforced concrete structures. During winter, the rate of corrosion increases as the structure is exposed to deicing salt from the vehicles. Figure 3-1 represents the roof level of the parking deck filled with snow after a winter storm.

Figure 3-1: Roof of the Lincoln Parking Deck filled with slushy snow.

Since the parking deck falls under Zone 3, i.e., it will be exposed to severe deicing chemicals. Inorganic salts, such as sodium chloride, magnesium chloride or calcium

chloride are the most common types of deicing salts. They are weak salts and have minimal effect on concrete. However, concentrated solutions of these salts can degrade the concrete (Cody et al., 1996). The study conducted by Cody et al., (1996) suggested that the use of deicing salts such as magnesium chloride is harmful when used on the concrete surfaces. Magnesium chloride reacts with calcium silicate hydrates found in the concrete and this result in the formation of magnesium silicate hydrates, leading to the weakening of the strength of concrete causing structural deterioration. Salts such as calcium chloride, dissolves oxygen and hydrogen ions present within calcium hydroxide found in concrete. This leads to cracking and crumbling of the structure.

3.2.2. Chloride ingress

Deicing salt is considered as the main constituent for initiating chlorination. Chloride ions dissolved in water can pass through the cracks or pores by capillary action of concrete and reach the rebar. Corrosion caused due to chloride ingress at the joints of two double T-beams is shown in Fig. 3-2.

Figure 3-2: Corrosion due to chloride ingress at the joint of two double T-beams.

Some researchers have claimed that chloride ions are mainly responsible for the corrosion of reinforcing steel in concrete. The higher the presence of chloride ions, the higher are the risks for metal corrosion (Ann and Song, 2007). If the amount of chloride ions present on the surface exceeds the critical limit before the initiation of corrosion, it is called as the chloride threshold limit (CTL). There are two types of corrosion agents available in the presence of chloride ions. The first one is water-soluble chloride, which is responsible for most corrosion. The second one is acid-soluble chloride, which is bound by the aggregates or cement and prevents the formation of corrosion.

Based on the composition of concrete, Clear and Hay (1973) suggested the conversion factor from acid-soluble chloride to water- soluble chloride to be between 0.35 and 0.90. According to their research, an arbitrary value of 0.75 was chosen and this resulted in a water-soluble chloride limit of 0.15% by weight of cement. After conducting various experiments on concrete, the Federal Highway Administration (FHWA) recommended a threshold limit of 0.20% acid-soluble chloride by weight of cement. Cement with higher chloride content instigates corrosion on bridge decks but, acid-soluble chloride is bound within the aggregates, thus most corrosion is caused by water-soluble chloride (Clear, 1976).

Chloride Threshold Limit has a critical impact on the service life of reinforced concrete structures (Ann and Song, 2007). The research conducted by Ann and Song (2007) on the CTL for corrosion of steel in concrete, proposed the CTL based on the physical conditions of the steel-concrete mix. The entrapped air voids present within the concrete were found to be more influential than the chloride binding e.g. acid chloride and the cement concrete binders. The anodic dissolution reaction of iron with higher pH in the

absence of chloride ions is represented in Eq. 3.1. This reaction is balanced by the cathodic reaction represented in Eq. 3.2. This process leads to the electrochemical reaction, where the Fe^{2+} ions combine with the hydroxyl ions and disrupts the passive film, thus destabilizing the steel reinforcement.

$$Fe \rightarrow Fe^{2+} + 2e^{-} \tag{3.1}$$

$$1/2O^{2} + H_2O + 2e^{-} \rightarrow 2OH^{-} \tag{3.2}$$

Studies suggest that the complete mechanism of the rupture of passive film by the chloride ions is difficult to analyze as the passive film is a thin layer (Rodriguez et al., 1997; Hansson et al., 2012). This is not a uniform process thus the formation of the anodic area where a majority of the corrosion takes place is considered as a local reaction while the rest of the steel remains in the passive state (Farny and Kosmatka, 1997).

Another research states that there is severe competition involved between chloride and hydroxide ions to combine with Fe^{2+} cations (Farny and Kosmatka, 1997; Hansson et al., 2012). This results in a reaction between Fe^{2+} cations and chloride ions, resulting in soluble complexes with Fe^{2+} ions. This slows the process of the formation of passive film and helps in the dissolution of metals. At this stage, the iron-chloride complex becomes soluble and drifts away from the reinforced steel surface resulting in the formation of corrosive products. At the same time, the free chloride ions go back to the anode to react with the steel. The hydroxyl ions are being constantly consumed during this reaction. This process intensifies the metal dissolution by decreasing the pH levels in the concrete (Farny and Kosmatka, 1997; Hansson et al., 2012).

3.2.3. Carbonation

The Carbon dioxide found in the environment reacts with the calcium hydroxide present in the concrete, resulting in the formation of calcium carbonate. This reaction is described by Eq. 3.3.

$$Ca(OH)_2 + CO_2 \rightarrow CaCO_3 + H_2O \quad (3.3)$$

This reaction decreases the pH below 8.5. Acidic gases such as sulfur dioxide (SO_2) and nitrogen dioxide (NO_2) lowers the pH in the concrete. Low pH values may lead to instability in the passive film. Carbonation is a slow process when compared to chlorination. According to Portland Cement Association (PCA, 2000), in high quality cement concrete, the rate of penetration of carbonation into concrete is estimated to be about 1.0 mm (0.04 in.) per year (PCA, 2002) as the humidity increases from 25% to 50%.

Before constructing the structure, the properties of concrete such as high water cement ratio, low cement content, shorter duration for curing, low strength or high permeability must be given importance as they lead to an increase in carbonation (ACI 330R, 2001; PCA, 2002). The chances of carbonation are higher when relative humidity is between 50% and 75%.

As the relative humidity drops to 25% and below, the chances of carbonation are low, hence they are negligible. At a higher relative humidity of 75% or above, the moisture within the pore structure of the concrete obstructs the entry of carbon dioxide (ACI 201, 1992). Carbonation-induced corrosion is more common in the building facades. These facades are unprotected from rainfall, shaded from sunlight and also has very minimum

concrete clear cover over the reinforcing steel, thus leading to carbonation of the structure (ACI 330R, 2001).

A chemical test is conducted to confirm the presence of carbonation on concrete surfaces. A small amount of Phenolphthalein when applied on the carbonated surface indicates the presence of carbonation. If the surface turns pink, it indicates the absence of carbonation. The presence of carbonation is confirmed if the surface turns colorless from pink (Bertolini et al, 2004). This experiment was performed on the parking deck to study the presence of corrosion due to carbonation. Figure 3-3 depicts the presence of carbonation on Level 1-D obtained from the exposed specimen which had fallen off the walls. This specimen was estimated to be no longer than a few weeks old. Figure 3-4 indicates the absence of carbonation on the unexposed surface of the specimen obtained from the same location.

Figure 3-3: Presence of carbonation detected as the concrete turns colorless.

Figure 3-4: Absence of carbonation indicated as the surface becomes pink.

3.2.4. Inadequate concrete clear cover

The depth of concrete clear cover provides protection against various environmental conditions. Appropriate depth must be provided for reinforcement on the top or side concrete covers. This is required for the durability of the structure (ACI 362.1R, 1997). The depth of concrete cover has to be provided in accordance with the rate of corrosion pertaining to that area. Both concrete cover and water-cement ratio are factors responsible for providing protection against corrosion. Studies suggest that a concrete cover of 25 mm (1 in) was ineffective against corrosion even with a low water-cement ratio of 0.28. The concrete cover was later redesigned with an additional 25 mm (1 in) thickness of silica fume (ACI 201, 1992; ACI 362.1R, 1997).

Figure 3-5 shows the formation of corrosion observed on the barrier walls in Level 1-D. Table 3-1 indicates the depth of concrete clear cover provided in the structure according to the details obtained from the structural drawings.

Figure 3-5: Corrosion observed on the barrier wall in Level 1-D.

Table 3-1: Depth of concrete clear cover (in) derived from the structural drawings

Description	Concrete Cover (in)	Protection
Beams Top Reinforcing	3	Uncoated
Beams Bottom Reinforcing	2	Uncoated
Beam Stirrups at Side and Bottom	1½	Uncoated
Beam Stirrups at Top	2½	Uncoated
Slab Top Reinforcing	2	Uncoated
Slab Bottom Reinforcing	1	Uncoated
Walls Not in Contact with Earth	1½	Uncoated

According to the structural drawings, the stirrups present at the side and bottom of the beams and for walls not in contact with earth had 1½ in. concrete clear cover was provided. During the investigation, the presence of corrosion was observed at the locations with inadequate concrete clear cover. During the visual inspection, the clear covers at various locations were inspected and it was observed that in places where 1½ in. was mentioned in the structural drawings only 1in. was provided. Areas which mentioned 2½ in. concrete clear cover showed only 2 in. when measured. This is clearly not sufficient to avoid corrosion as Ohio falls under Zone -3/CC- II (ACI 318, 2002; ACI 362.1R, 2002).

Figure 3-6 represents the image of the exposed steel reinforcements on the walls of the deck with an average clear cover of about 0.6 in. Adequate clear cover should be provided as carbonation or chloride ingress reduces the strength of concrete and reaches the reinforcement bars causing corrosion (Glass et al., 1991).

Figure 3-6: Inadequate concrete cover seen on the outside of the exterior walls.

3.2.5. Water leakage

This is one amongst the most ignored category when it comes to the construction of parking decks. Routine maintenance might give early indications on the issues caused due to water leakage. Figure 3-7 shows rust stains on the columns because of water leakage. Neglecting this issue would result in necessary repairs in the future.

Figure 3-7: Corrosion stains caused due to water leakage.

Three major signs of a water leakage in a concrete structure are rust stains on the walls, efflorescence and metal rusting from parts that are not covered (Western Specialty Contractors, 2015).

3.2.6. Freeze-thaw cycles

The expansion of water is about 9% when it freezes. As the pore water within the pores and capillaries freeze, it exerts a pressure. When this pressure exceeds the tensile strength of concrete, it causes ruptures leading to the formation of cracks within the concrete. The

constant cycles of freezing and thawing can eventually subject the concrete to significant expansion and contraction, cracking, scaling and spalling (PCA, 2002). Due to the presence of larger pores concrete has a higher capacity for water intake (Zhang et al., 2017). Experiments such as Accelerated Steel Corrosion Test, Bond-Slip test for concrete suffering the coupling action of freeze-thaw damage and steel corrosion helps in the determination the effects of freeze-thaw cycles on corrosion (Mu et al., 2002; Zhu et al., 2016).

3.2.7. Traffic surfaces

Upon inspection, the amount of vehicular traffic on the parking deck has caused considerable amount of wear to the structure. During winter, the abrasive nature of the tire chains and snow studded tires has resulted in the loss of concrete from the surface. Figure 3-8 shows the surface of the deck which has undergone wear because of vehicular movements.

Figure 3-8: Wear and tear caused from tires of the vehicles.

When the metals present on studded snow tires come in contact with the surface it leads to flailing or scuffing. The compressive strength of concrete is mostly sufficient to resist abrasion but also highly dependent on the aggregate abrasion properties. Higher the compressive strength, higher is the abrasion resistance of the concrete (PCA, 2002).

3.2.8. Surface defects

Surface defects occur due to poor materials and improper construction practices. The most commonly found defects on the surface of the structures are formed due to the entrapment of air bubbles present within the concrete, known as surface air voids or bug holes. Low workability, excessive fine aggregate content, uncontrolled use of form releasing agent or use of vibrators with high amplitude could also be responsible for the formation of surface defects. The main reason for air voids is lack of consolidation. The typical width of a bug hole ranges between 15mm and 25 mm (PCA, 2002). In Fig. 3-9, the minimum width of a bug hole was found to be about 2mm and the maximum was around 26mm.

Figure 3-9: Bug holes found on the slabs.

Chapter 4. Experimental Methods, Results and Discussion

The residual integrity of concrete structures is coupled with the effects of deterioration due to physical and chemical processes (Cigna et al., 2003). Non-destructive testing methods were used to prevent further deterioration of the structure during evaluation. A structural assessment was performed based on the information obtained from Ground Penetrating Radar, SIR 4000 and the data obtained from probabilistic models.

4.1. Assessment Procedures

The following sections explain the procedure used in identifying corrosion and assessing the structural health of the Lincoln Parking Deck.

4.1.1. Structural drawings

The first step of the assessment was to review the structural drawings of the parking deck provided in Appendix A. The structure was designed and constructed in the 1970's, and many of the precast structural drawings with important detailing could not be located. However, the Facilities Management Services at YSU provided the available structural and constructional drawings. Under the general notes section, details about size and type of reinforcement such as uncoated, epoxy-coated or galvanized were mentioned. Other details, such as pre-stressed or post-stressed, drainage, electrical and plumbing were also given in the drawings. The drawings also include an overview of the repair history of the structure, in particular where and when the renovations took place.

4.1.2. Visual inspections

This step was important in documenting the areas of corrosion on the structure. A series of photographs were taken to record the path of corrosion at various locations. These photographs were used to conduct a detailed study into the types of corrosion mentioned in Section 2.4. The bright brownish colored stains on the columns (as seen in Fig. 4-1) and exposed reinforcement bars due to lack of concrete clear cover were a few amongst the many identified corrosion spots during the visual investigation.

Figure 4-1: Corrosion stains on the columns at Lincoln Parking Deck.

4.1.3. Non-destructive testing

The non-destructive testing was conducted using an SIR 4000 and Profoscope. The SIR 4000 equipment was the basis for mapping areas with visible corrosion. The data obtained from the SIR 4000 was processed using RADAN software. This step was

necessary to assess the reinforcement details, including rebar size and the depth of concrete clear cover which were measured using the SIR 4000 and Profoscope.

4.1.3.1. Ground Penetrating RADAR (GPR)

Ground Penetrating RADAR (Radio Detection And Ranging) is one of the latest available methods to detect corrosion in embedded reinforcing steel, mainly delamination. GPR utilizes Ultra-Wide Band (UWB) energy, which provides a wide range of frequencies. The GPR has low power emissions compared to other electromagnetic devices, typically about 1% of the energy emitted from a cellphone. A typical GPR is shown in Fig. 4-2. The GPR functions by propagating a wide range of electromagnetic frequencies through the depth of the specimen for both metallic (steel) and non-metallic components (pipes) (SIR 4000 Manual, 2016).

Figure 4-2: A perspective view of the GPR SIR 4000.

The result is then processed by the software to obtain the necessary details about the depth, clear cover, spacing of the rebar and presence of voids within the concrete structures are typically comprised of different structural components using various materials with different dielectric constants. The GSSI manual has specified the values for dielectric constants based on different surface conditions. For instance, the dielectric constant of air and water are 1 and 81, respectively.

The dielectric constant plays an important role in attaining the required data of the surface as it travels at different speeds depending on the material it passes through. The speed is not considered as constant. If the ratio of dielectric constants between two materials at an interface is larger, the reflection obtained is stronger thus making the target much brighter, and vice-versa. The concrete itself can have different variations in its dielectric constants depending on hydration age, porosity or moisture state. Based on the type of surface, a set of values were pre-installed in the GPR by the manufacturers. This helped in identifying the di-electric constant pertaining to the specific surface. In this research, the dielectric constant for concrete was between 6 and 6.5 as the hydration age of the concrete was much greater than 1 year at the time of the experiment. The dielectric constant for concrete typically ranges between 4 and 11 (SIR 4000 Manual, 2016).

The testing frequency range also influences the reliability of the data. According to the SIR 4000 Manual (2016), lower frequencies results in higher resolutions. The 1.6 GHz antenna was used to map the areas of corrosion on the Lincoln Parking Deck due to the increased depth range of 18 inches. The areas of the parking deck where maximum deterioration was observed during visual inspection were scanned using the GPR. The

data was then processed using RADAN 7 software. This software helped in mapping the reinforcement condition (along the entire section).

Table 4-1 gives a comparison between 2.6 GHz and 1.6 GHz antennas available on the SIR 4000 GPR (SIR 4000 Manual, 2016). The GPR operates with an UWB frequency range either in in MHz (Million Hz) or in GHz (Billion Hz). The SIR 4000 has 2 antennas with 1.6 GHz and 2.6 GHz, which can be used for scanning in different conditions.

Table 4-1: Comparison between 2.6 GHz and 1.6 GHz Antennas

Antenna	2.6 GHz (Model 52600S)	1.6 GHz (Model 5100S)
Penetration Depth in	10 inches	18 inches
Range	8 ns	12 ns
Samples per Scan	512	512
Resolution	32 bits	32 bits
Number of gain points	4	5
Vertical High Pass Filter	500 MHz	250 MHz
Vertical Low Pass Filter	4000 MHz	3000 MHz
Scans per second	100	100
Vertical IIR High Pass	10 MHz	10 MHz
Transmit Rate	100 KHz	100 KHz

4.1.3.2 Profoscope

Due to the size of the GPR apparatus, it was not convenient to be used in all areas such as stem of the T-beam and walls. To overcome this limitation, a Profoscope was used. The dimensions of this equipment were about 7½ in. (190.5 mm) in length and 3 in. (76.2 mm) in width. The Profoscope works on the principle of electromagnetic pulse induction

technology. The electric current present within the rebar is detected by the Profoscope via eddy currents induced by a magnetic field in the opposite direction of the current (Proceq, 2009). The change in voltage is correlated to rebar size and the strength of the current is correlated to cover depth. The Profoscope was also used to determine the depth of concrete clear cover and reinforcements in several areas. The instrument had to be calibrated before the experiment. This was done using the knob on the upper side of the instrument. Figure 4-3 depicts the Profoscope being used to determine the depth of concrete clear cover on the exterior walls of the parking deck.

Figure 4-3: The Profoscope being used to determine the depth of concrete clear cover on the wall.

4.2. Deterioration Phases

The service life of a structure is typically classified into two categories as shown in Fig. 4-4, initial and propagation phases (Duracrete, 2000). The primary cause of deterioration in the initial phase is the development of cracks along the structure. These cracks allow

the ingress of chloride and accelerate the onset of corrosion. At this stage, the reinforcement reacts to the surroundings causing de-passivation of the outer layer.

The second phase is the propagation phase. The propagation phase is typically divided into three sub categories. They are as follows: the approximate time since the inception of corrosion (T_i); the approximate time for visible crack formation, which is simply known as the propagation period (T_p); and the approximate time for the cracks to expand, leading to further deterioration of concrete (T_d); after which the structure fails. All these factors are combined to predict the functional service life (T_f) of the reinforced concrete structure (Duracrete, 2000; Hájková et al., 2016; Hartt et al., 2004). These phases are explained in more detail in the next Section 4.2.1 onwards.

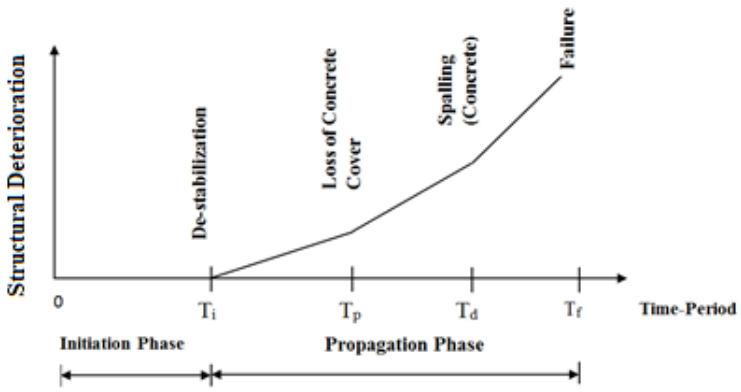

Figure 4-4: Graphical representation of the deterioration phases (Duracrete, 2000).

4.2.1. Chlorination during propagation phase

A probabilistic corrosion model based on research conducted by Liu and Weyers' (1998) provides an ideal depiction of the relationship between corrosion current density (i_{corr}) and ohmic resistance (R_C) for chlorides. The use of current density has been widely used

to determine the durability of concrete (Liu and Weyers, 1998; Sadowski and Nikoo, 2014). The typical definition of Ohm's law states that, Ohmic resistance (Rc) is inversely proportional to the corrosion current density (Fleming and Ambrose, 1911). As the current is introduced into the material, there is a presence of strong force acting against this current, or resistance (Millikan and Bishop, 1917).

As the corrosion current density increases, the ohmic resistance decreases. The values of Ohmic resistance (R_C) for the results presented herein were obtained from Eq. 4.1. The maximum chloride ion content (C_t) was taken as 0.06, 0.15 and 0.30 as mentioned in the structural drawings. The average temperatures (T) between 1970 and 2016 were obtained from National Centers for Environmental Information and are tabulated in Table 4-2. The time interval (t) was taken as 5 years from 1971 to 2016. These data were then used to determine the rate of change of corrosion density on the Lincoln Parking Deck. Using MATLAB, Eqs 4.1 and 4.2 were evaluated, plotted and summarized in Fig. 4-5.

$$R_C = exp[8.03 - 0.549\ ln(1+1.69C_t)] \quad (4.1)$$

$$i_{corr} = 0.926.exp\ [7.98+0.7771\ ln\ (1.69C_t) - (3006 / T) - 0.000116R_C + 2.24t^{-0.215}] \quad (4.2)$$

The general trend in Fig. 4-5 indicates that as the maximum chloride ion content increase, corrosion current density increases showing the initiation of chloride-induced corrosion. Based on the assumed values, the highest corrosion current density was seen in 2011 as the average temperature in 2011 was recorded as 75° F (297.039 K) when compared to the other years.

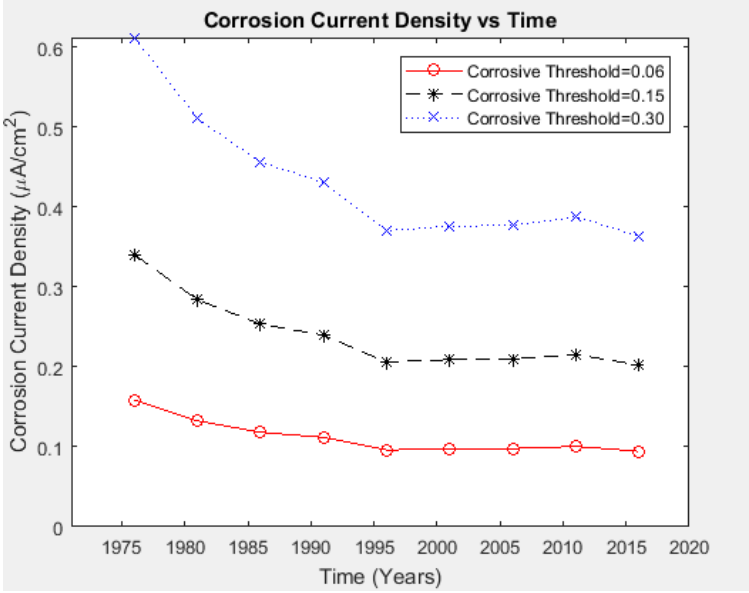

Figure 4-5: Corrosion current density (μA/cm2) vs. time (years).

The results in Fig. 4-5 indicate the rate of current density which was initially higher, slowly started decreasing after 1975, after which the change in corrosion current density stabilized. This is due to the steel remaining in its passive state as de-passivation of the reinforcement had not taken place yet.

A few years after 1975, the rate of current density starts decreasing indicating a potential for reinforcement corrosion to occur. The current density stabilizes after 1995, indicating depassivation of steel reinforcement. This has been recorded in Table 4-3. Based on the values obtained from the chlorination model, the rate of corrosion current density for the parking deck is 0.388 μA/cm^2 for a maximum chloride ion content of 0.30. The rate of corrosion is classified between low and moderate for a corresponding corrosion penetration depth rate between 2 and 6 μm/year (Millard, 2003).

Table 4-2: Average Temperature between 1971 and 2016

Year	T(years)	Avg. Temperature	Avg. Temperature
1971	0	69	293.706
1976	5	69	293.706
1981	10	71	294.82
1986	15	71	294.82
1991	20	72	295.372
1996	25	67	292.594
2001	30	70	294.261
2006	35	72	295.372
2011	40	75	297.039
2016	45	73	295.928

Table 4-3: Corrosion Current Density

Time (Years)	Max. Cl^- Content		
	0.06	0.15	0.30
1971	∞	∞	∞
1976	0.159	0.341	0.612
1981	0.133	0.2843	0.5111
1986	0.118	0.254	0.406
1991	0.112	0.240	0.431
1996	0.096	0.206	0.307
2001	0.098	0.209	0.376
2006	0.097	0.210	0.377
2011	0.106	0.216	0.388
2016	0.094	0.202	0.364

4.2.2. Corroded steel during propagation phase

Chlorination and Carbonation corresponds to the total amount of corrosion in the structure. As discussed earlier in Section 3.2, concrete reacts with carbon dioxide releasing by-products that cause harmful effects on the structure. Carbonation mainly affects the porosity of concrete causing shrinkage and cracking of the structural elements (Šavija and Lukovic, 2016). The rate of carbonation in the structure is calculated using the basic principle of Faraday's Law of Induction, which states that the induced electromotive force within a closed circuit is equal to the negative of the rate of change of time of the magnetic flux (Jordan et al., 1968).

The average corrosion rate due to carbonation or chlorination in the radial direction (x_{corr}) is represented by Eq. 4.3 (Rodriguez et al., 1996). The type of corrosion is determined by a parameter called $R_{corr.}$ According to the studies conducted by Darmawan and Stewart (2007), the values of R_{corr} are taken as 1 for chlorination and as 5.5 for carbonation. In this case, the total time (t) is taken from 1971 to 2016. By integrating Eq. 4.4 using MATLAB, the total amount of corroded steel (X_{corr}) in radial direction (mm) is obtained.

$$x_{corr}(t) = 0.0116 i_{corr}(t) \tag{4.3}$$

$$X_{corr}(t) = \int_{t_{int}}^{t} 0.0116\ i_{corr}(t)\ R_{corr}\ dt \tag{4.4}$$

These results further helped in understanding the combined effects of both chlorination and carbonation on the rebar. These results obtained from the model, show that as the total chloride content present in the concrete increases, the total amount of corroded steel also increases. Table 4-4, contains values for different amounts of maximum chloride ion present in various elements of the structure such as slabs, beams and columns as given in

the structural drawings. Figure 4-6 depicts the total amount of corroded steel in radial direction (mm) due to the combined effects of carbonation and chlorination on the structure from 1971 to 2016.

Table 4-4: Corroded steel (Xcorr) in radial direction (mm) for Chlorination and Carbonation

Case	Max. Cl^- Content	Total Chloride Content	Carbonation (mm)	Chlorination (mm)
1	0.06	0.2136	0.0102	0.0563
2	0.15	0.5339	0.0219	0.1206
3	0.30	1.0679	0.0394	0.2169

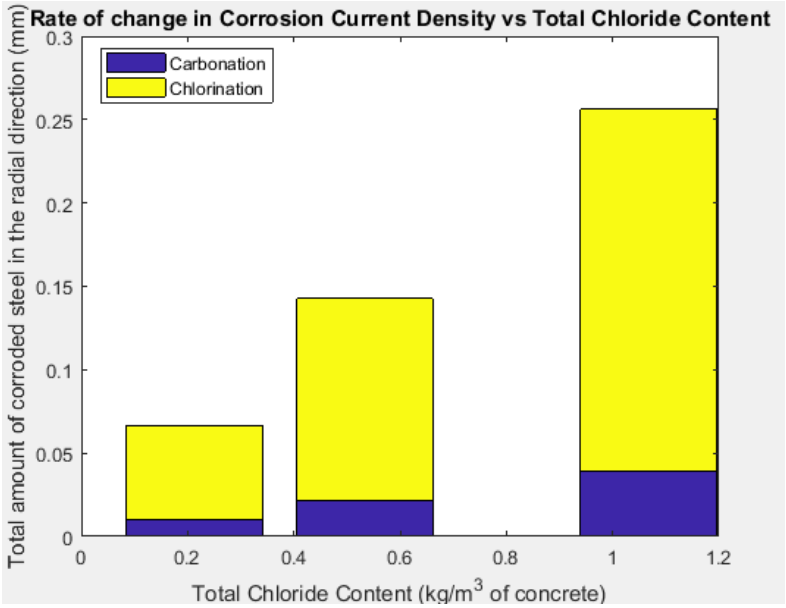

Figure 4-6: Rate of change in corrosion current density (μA/year) vs. total chloride content (kg/m^3 of concrete).

According to the results obtained from the probabilistic corrosion model shown in Table 4-4, Case-3 has a higher probability of undergoing chlorination than carbonation with the

maximum chloride ion content of 0.30. As per the results obtained from Case-3, the amount of chlorination is 81.83% higher than carbonation.

Equation 4.5 was used to calculate the evolution of the bar diameter. Based on the structural drawings, the most commonly used bars were ½ in. diameter seven-wire strand for the prestressed sections, #5, #8 and #9 bars. Although carbonation also attacks the reinforcement, chlorination causes more deterioration. Based on the test results and the data obtained from corrosion models, prestressed double T-beams with ½ in. diameter seven-wire strand were considered for observations. For a maximum chloride ion content of 0.30, the reduced bar diameter for ½ in. seven-wire strand was determined as 0.4969 in. and 0.4829 in. with respect to both carbonation and chlorination. These data are tabulated in Table 4-5.

$$d(t) = d_{ini} - \Psi\, 2x_{corr}\,(t) \tag{4.5}$$

Table 4-5: Evolution of bar diameter (in)

Max. Cl^- Content	Diameter of rebar, d_{ini} (in)							
	½ in. 7-wire		0.625 (#5)		1.0 (#8)		1.128 (#9)	
	C (in)	Cl(in)	C(in)	Cl(in)	C(in)	Cl(in)	C(in)	Cl(in)
0.06	0.4992	0.4956	0.6242	0.6206	0.9992	0.9956	1.1272	1.1236
0.15	0.4983	0.4905	0.6233	0.6155	0.9983	0.9905	1.1263	1.1185
0.30	0.4969	0.4829	0.6219	0.6079	0.9905	0.9829	1.1249	1.1109

4.2.3. Cracking of concrete cover

Concrete has poor tensile strength and the necessary tensile strength is provided by steel reinforcement. Cracking on structures is often inevitable when tensile stresses develop.

Due to evaporation of water from the surface, plastic shrinkage can occur and leads to the formation of cracks on the surface. This can be caused by low humidity and inadequate curing. Cracks can also form due to tensile strains induced by settlement (Zhang et al., 2010). Surface cracks are the portal to structural deterioration.

As cracks begin to develop, the ingress of chloride ions and other chemicals into the concrete accelerates leading to corrosion in reinforcing steel. The final technical report of Duracrete (2000) suggested Eq. 4.6 for the estimation of the critical horizontal crack width of corroded steel due to cracking of concrete ($x_{corr,cr}$) caused by carbonation and chlorination, which was based on the horizontal cracking of concrete clear cover. The depth of concrete clear cover was represented as C (m). According to the final technical report by Duracrete, parameters a_1, a_2 and a_3 were given as 7.44e-5 (m), 7.30e-6 (m) and -1.74e-5 (m/MPa), respectively. The characteristic splitting tensile strength of concrete ($f_{t,ch}$) was calculated for a compressive strength of 5 ksi (35 MPa) as mentioned in the structural drawings.

$$x_{corr,cr} = a_1 + a_2 (C / d_{ini}) + a_3 f_{t,ch} \tag{4.6}$$

Equation 4.6 was analyzed in MATLAB using 4 different rebar diameters (d_{ini}) such as ½ in. seven-wire strand, #5, #8 and #9 bars with a clear cover thickness of 1 in.,1.5 in.,2 in.,2.5 in. and 3 in., obtained from the structural drawings. Table 4-6 shows the corresponding values for different diameters of reinforcement after corrosion modelling.

Table 4-6: Critical horizontal crack width in the clear cover (cracking), xcorr,cr (m)

Cover, C		Diameter of rebar, d_{ini} (m)			
(m)	(in)	½ in. 7-wire strand	#5	#8	#9
0.0254	1	0.0481	0.0408	0.0300	0.0279
0.0381	1.5	0.0662	0.0553	0.0390	0.0359
0.0508	2	0.0843	0.0698	0.0481	0.0440
0.0635	2.5	0.1024	0.0843	0.0571	0.0520
0.0762	3	0.1205	0.0987	0.0662	0.0600

Based on the results obtained from the corrosion model shown in Fig. 4-7, it was observed that the critical horizontal crack width of corroded steel in concrete increases with the increase in the depth of concrete clear cover. Although, the purpose of concrete clear cover demands it to stop the ingress of chlorides into the concrete, it often contradicts this statement. As the thickness of the concrete clear cover increases, occurrence of cracks on the surface is more likely (Berkowskia et al., 2013).

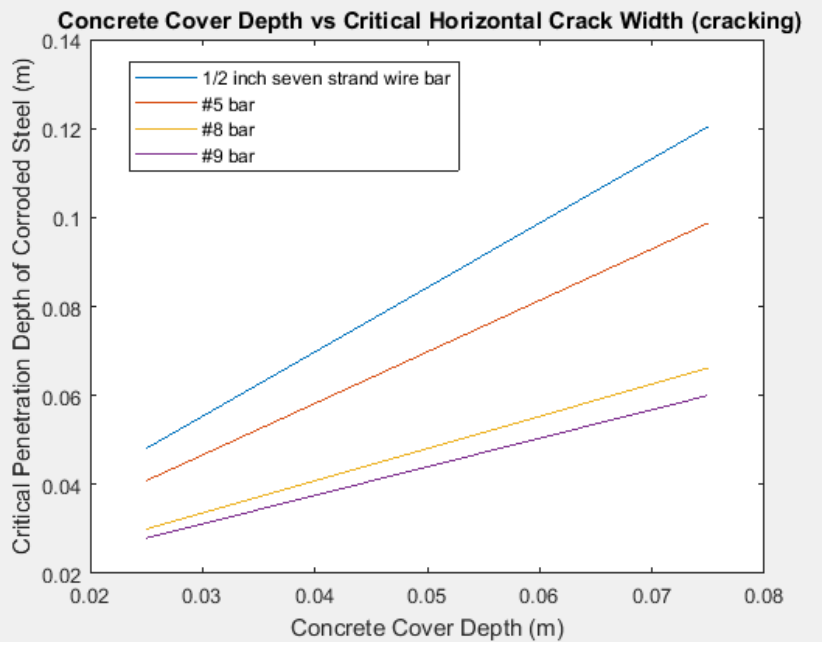

Figure 4-7: Concrete cover depth (m) vs. critical horizontal crack width in the clear cover (cracking), xcorr,cr (m).

It was also observed that the values of critical horizontal crack width for ½ in. diameter seven-wire strand are higher when compared to other reinforcements. Thus, for ½ in. diameter seven-wire strand, the critical horizontal crack width of corroded steel in concrete ($x_{corr,cr}$) is obtained as 1.89 in. (0.0481 m) with a concrete clear cover depth of 1 in. (0.0254 m) and 4.7 in. (0.1205 m) with a concrete clear cover depth of 3 in. (0.0762 m). The results indicate a 59.78% increase in the depth of corrosion in steel for cracking in the horizontal direction as the concrete clear cover increases from 1 in. to 3 in.

4.2.4. Spalling of concrete cover

The last and final stage of deterioration in the propagation phase is spalling. Spalling is usually represented by circular or oval depressions with depths ranging between 1 in. (25

mm) and 6 in. (150 mm) (PCA, 2000). At this stage, the reinforcement may be directly exposed to water and chlorides, accelerating corrosion and often leading to failure.

During the investigation, no signs of spalling were observed on the structure except in two or more locations. Although, there were certain locations which indicated the occurrence of spalling on the structure however these locations were repaired during the 2012 renovations, as shown in Fig. 4-8. Proper care must be taken before the onset of spalling on the concrete surfaces.

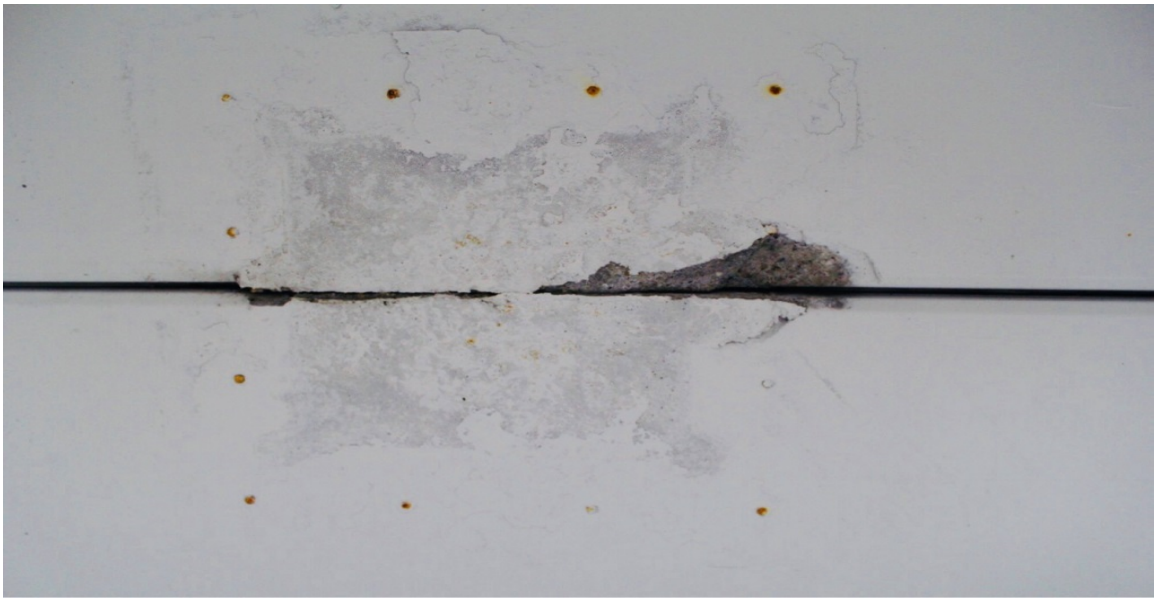

Figure 4-8: Repaired section of the Lincoln Parking Deck showing signs of spalling.

To analyze the attack of spalling on the surface, Hájková et al., (2016) suggested Eq. 4.7.

$$x_{corr,sp} = ((w^d - w_0)/b) + x_{corr,cr} \quad (4.7)$$

As per the studies conducted by Hájková et al., (2016), the critical crack width (W^d) for spalling was given as 1mm (0.039 in.). For the analysis of this corrosion model, width of initial crack (W_0) was obtained from on-site experiments, conducted using an optical

comparator. The values for initial crack width (W_0) were obtained from spots with visible cracks in the horizontal direction and were found to be 0.2 mm (0.0002 m), 0.5 mm (0.0005 m), 0.7 mm (0.0007 m), 0.75 mm (0.00075 m) and 0.9 mm (0.0009 m), respectively.

Equation 4.7 was calculated in MATLAB using the values obtained from the critical horizontal crack width of corroded steel in cracking, $x_{corr,cr}$ from the previous corrosion model shown in Table 4-7. Seven-wire strand with ½ in. diameter and #9 reinforcement were used to determine the critical horizontal crack width of corroded steel with a concrete cover depth of 1.5 in. (0.0381 m) and 2 in. (0.0508 m) as the structural components involving these reinforcements might undergo spalling in the future as per the investigation. Equation 4.7 estimates the critical horizontal crack width of corroded steel due to spalling ($x_{corr,sp}$) for both carbonation and chlorination with respect to the position of reinforcement, given as b. The value of b is taken as 8.6 μm/μm and 10.4 μm/μm for top and bottom reinforcement, respectively. Tables 4-7 and 4-8 represent the evaluation of Eq. 4.7 to obtain the critical horizontal crack width of corroded steel in spalling.

Table 4-7: Critical horizontal crack width in the clear cover (spalling), xcorr,sp (m)for top reinforcement

$x_{corr,cr}$ (m)	W_0 (m)				
	0.0002	0.0005	0.0007	0.00075	0.0009
0.0662	0.1431	0.1142	0.0950	0.0902	0.0758
0.0843	0.1612	0.1323	0.1131	0.1083	0.0939
0.0359	0.1129	0.0840	0.0648	0.0600	0.0456
0.0440	0.1209	0.0920	0.0728	0.0680	0.0536

Table 4-8: Critical horizontal crack width in the clear cover (spalling), xcorr,sp (m)for bottom reinforcement

$x_{corr,cr}$ (m)	W_0				
	0.0002	0.0005	0.0007	0.00075	0.0009
0.0662	0.1592	0.1243	0.1011	0.0952	0.0778
0.0843	0.1773	0.1424	0.1192	0.1133	0.0959
0.0359	0.1290	0.0941	0.0708	0.0650	0.0476
0.0440	0.1370	0.1021	0.0789	0.0730	0.0556

In Fig. 4-9, the general trend in the graph shows the lines decreasing with respect to the increase in initial crack width. The downward trend in the graph indicates that, as the crack width increases it becomes easier for the ingress of chlorides to reach the reinforcement.

It is further noticed that the critical depth can be attained easily with the increase in the width of cracks in the horizontal direction. From the trends observed in Fig. 4-9, both top and bottom reinforcements show similar data pattern based on the calculations. The results suggest the critical horizontal crack width required for the structure to undergo spalling and however must be checked occasionally for formation of cracks in the horizontal direction. If the crack width exceeds the critical values the spalled area must be repaired immediately to avoid further deterioration.

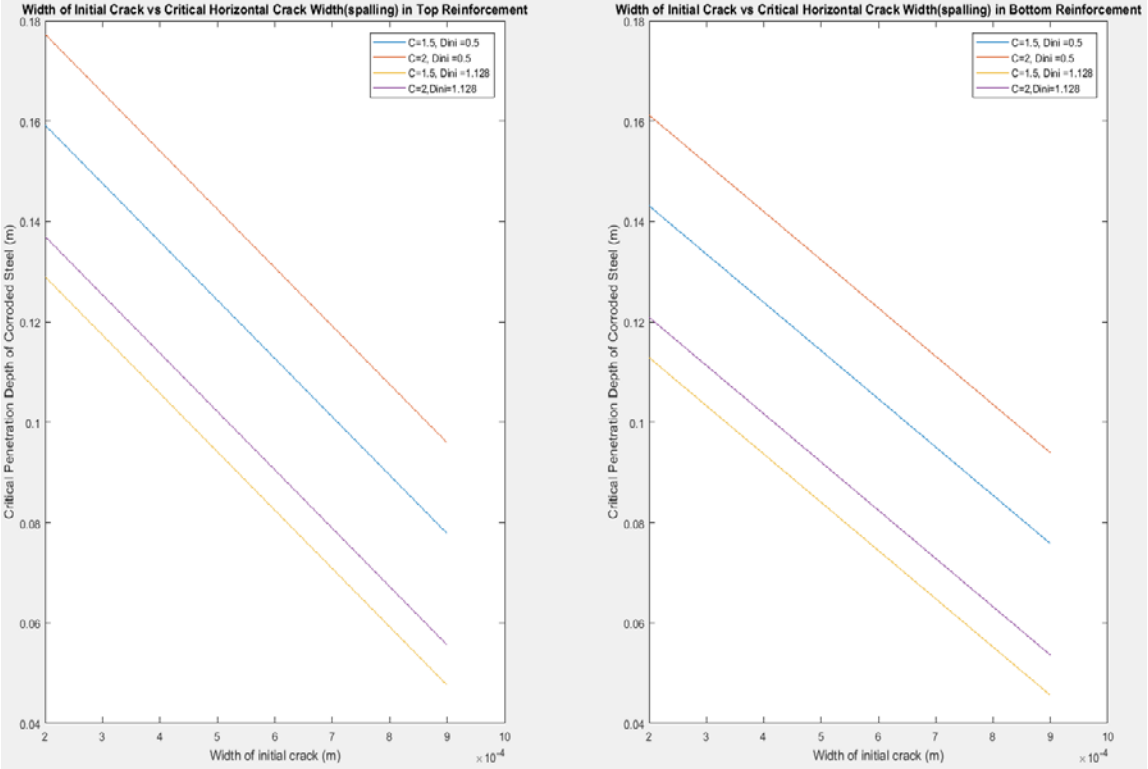

Figure 4-9: Width of initial crack (m) vs. critical horizontal crack width in the clear cover (spalling), xcorr,sp (m). for top and bottom reinforcement respectively.

4.3. Structural Analysis

A double T-beam section was analyzed to determine the behavior and capacity of the member. The parking deck consists of simply supported pre-stressed, precast double T-beam sections which are 9 ft. wide, 34 in. deep and 60 ft. in length as shown in Fig. 4-10. The design loads were calculated using the dead, live, snow and rain loads acting on the section as mentioned in the structural drawings.

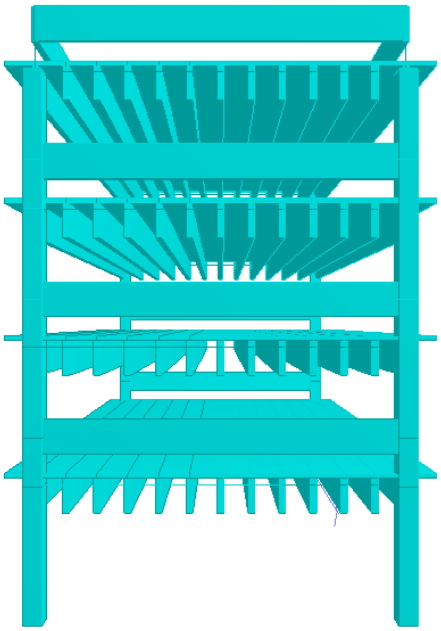

Figure 4-10: Animated view of the section of Lincoln Parking Deck from X-axis.

The structural analysis was performed based on the reinforcement details provided in the drawings and again using the current reduced reinforcement obtained from the scanning and deterioration phases. As the sections were pre-stressed, the initial yielding strength of the reinforcement bar was taken to be 270 ksi rather than the typical 60 ksi. It is a seven-wire strand with a diameter of ½ in. (12.7 mm) with a nominal area of 0.153 in^2 (98.07 mm^2).

Figure 4-11 shows the scanned portion of the slab from Level 4A with the diameter of the reinforcement being measured 0.5 in. In Fig. 4-11, the depth of the reinforcement is seen at 1.5 in. from the top. The white area indicates the presence of air and the sharp black lines are the reflections obtained from the reinforcements.

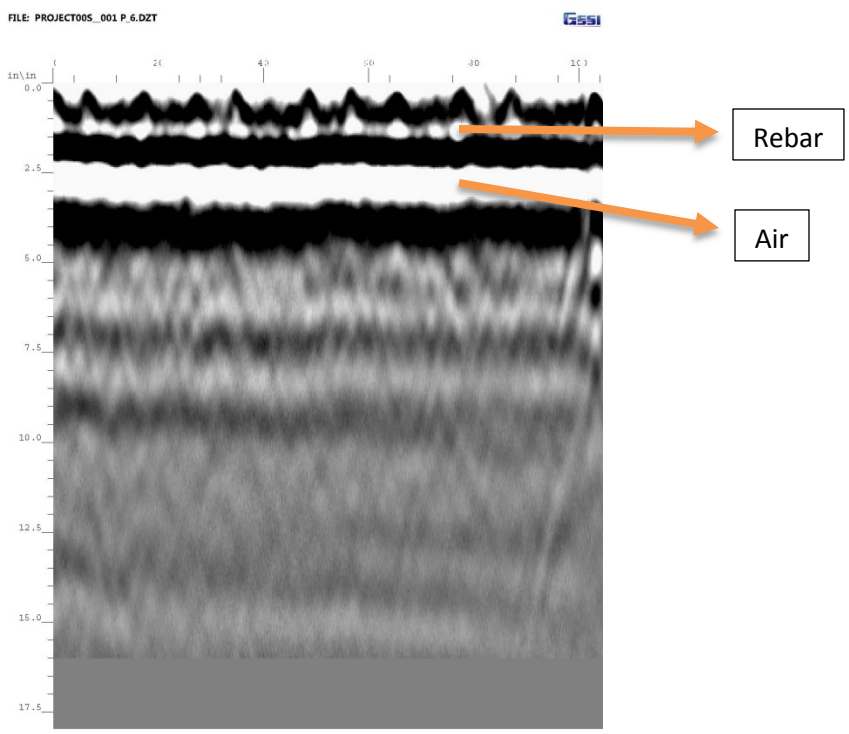

Figure 4-11: Section of the slab from Level 4A in Lincoln Parking Deck from RADAN.

A total of 15 sections were analyzed with extreme corrosion visible from the outside. Using Profoscope, the depth of concrete clear cover for the stem of the double T-beam was found to be 1.25 in. with an average diameter of 0.49 in. after corrosion with a standard deviation of 0.009. This is recorded in Appendix B.

In another case, Fig. 4-12 shows the scanned portion of the slab from Level 3B with an average diameter of the reinforcement being measured as 0.5 in with zero standard deviation. The section shown in Fig. 4-12 was analyzed and calculations were performed with respect to the initial and present conditions of the reinforcement collected from the results obtained from the probabilistic data for corrosion modelling.

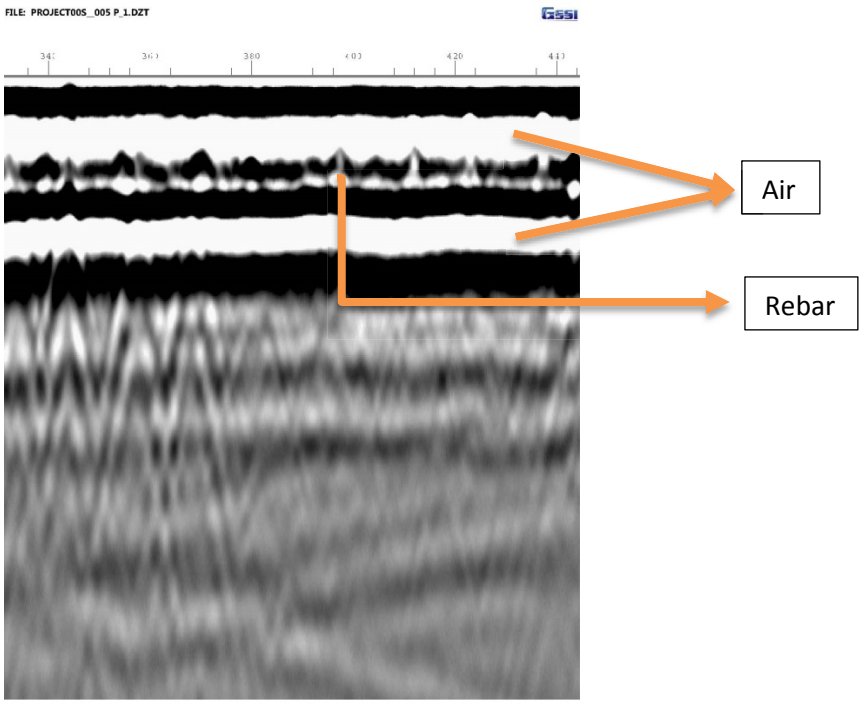

Figure 4-12: Section of the slab from Level 3B in Lincoln Parking Deck from RADAN.

According to the results for chlorination and carbonation modelling, the current diameter of the ½ in. seven-wire strand was estimated to be 0.4829 in. and 0.4969 in. respectively. The structural analysis was performed with the lowest residual diameter value of 0.4829 in. This resulted in a decrease of 4.24% of the total reinforcement area due to chlorination-induced corrosion. The results for the initial (i) and current (ii) conditions of the structure are tabulated in Table 4-9.

Table 4-9: Comparison of initial and current moment capacity and stresses in typical T-beam

ii. Initial Condition				
Due to loads		Strength of Materials		Remarks
M_u	285 k-ft	φM_n	1101.032 k-ft	ok
Stress in Steel	215.75 ksi	Strength of Steel	270 ksi	ok
Stress in Concrete	4.77 ksi	Strength of Concrete	5 ksi	ok

ii. Current Condition				
Due to loads		Strength of Materials		Remarks
M_u	285 k-ft	φM_n	1093.50 k-ft	ok
Stress in Steel	217.25 ksi	Strength of Steel	270 ksi	ok
Stress in Concrete	4.63 ksi	Strength of Concrete	5 ksi	ok

The results indicate that the capacity of the structure is satisfactory, thus being safe. The calculations for structural assessment are shown in Appendix C. Based on the results from structural analysis, the stress in reinforcing steel increased by 1.5 ksi due to the decrease in reinforcement area. Due to the presence of cracks, the compressive strength of concrete decreased from 4.77 ksi to 4.63 ksi, a difference of 0.14 ksi between the initial and current strength of concrete.

Chapter 5. Economical Remedies and Recommendations

Based on the studies conducted by various other researchers in the field of corrosion, a few economical solutions have been summed up to counteract the adverse effects of corrosion in structures. These methods are considered economical based on the availability and general construction use and have been suggested for both new and existing structures. Non-destructive testing of the existing structures is suggested as a means of maintaining the integrity of the whole structure.

5.1. Economical Remedies for Existing Structures

As the formation of corrosion takes place gradually over time, it is difficult to analyze the existing structures. Routine maintenance is the only method to detect corrosion in its early stages. Once the structure has been constructed, regular checks will reveal the activities of corrosion and one of the following economical remedies explained in the next section could delay the process of corrosion to some extent.

5.1.1. Penetrating sealants

Penetrating sealants penetrate the concrete surface and protect the steel reinforcement by obstructing the flow of chloride ions and water molecules. They are inexpensive and are readily available. They are typically made of silane and siloxane and allow the evaporation of trapped moisture through the exposed concrete surface as the sealants are vapor transmissive. The sealers can be applied by hand and the process is relatively economic. The effectiveness of the surface sealant decreases over time and it must be reapplied every five years to prevent corrosion (Teng et al., 2014).

5.1.2. Crystalline sealants

Crystalline sealants form a 3-D structure through the process of crystallization (Flores et al, 2016). On application, the crystals present in the sealant react with the water in the concrete. These crystals have strong self-healing properties which help in sealing cracks effectively (Krauss and Naus, 1998). They are typically used either as an admixture or applied directly onto the affected surface.

5.1.3. Impressed current cathodic protection

Impressed current cathodic protection (ICCP) is used when the galvanic anodes such an magnesium, aluminum and zinc cannot provide the required current to avoid corrosion. In this method, the electrochemical process is reversed by applying an electric potential through the reinforcement. An external power source provides the necessary current and proper care must be taken before mounting the ICCP in the parking systems (Christodoulou et al., 2010). Unnecessary current densities might cause reactions between the acids generated by the anodes and the concrete, leading to severe damages to concrete. While installing ICCP, the anodes must be spaced at less than a foot. The anodes must also be present throughout the structure as the distribution of current within the concrete is poor (Wilson et al., 2013).

5.1.4. Polymer impregnation

This process involves filling voids in concrete with the aid of a monomer. This often provides a tough layer which is almost impermeable against corrosion causing chloride ions. This requires heavy drying after application. Despite its toughness, this technique is vulnerable to frequent cracking after drying (ACI 548.1R, 1997). Also, due to excessive

costs, this method is often impractical. Studies are still going on in the field of Polymer-Impregnated Concrete to make it a viable economic remedy against the impregnation of chloride ions.

5.1.5. Migrating corrosion inhibitor

Migrating Corrosion Inhibitors (MCI) can be used as an admixture or can be directly applied to the surface of the existing structure using vacuum pressure injection methods, as they cannot reach the steel without an external pressure. After the application of MCI onto the surface, the MCI is absorbed into the concrete pores and reaches the reinforcing steel through capillary action. The ionic attraction of the inhibitor provides a protective coating on the steel reinforcement. It acts as a protective layer by chemically passivating the outer layer of reinforcement to slow corrosion. Calcium-nitrite based inhibitors are one of the most commonly used inhibitor (ACI 362.1R, 1997). The Lincoln Parking Deck makes use of this inhibitor. It was applied during the renovations in 2012. However, the use of MCIs on Lincoln Parking Deck did not show improvements in the reduction of corrosion.

5.2. Economical Remedies for New Structures

A review of various methods indicates the following remedies to be considered as most reliable. The availability of the product, effortless application, low investment and less time consumption were a few of the criteria analyzed to choose these remedies.

5.2.1. Cementitious capillary crystalline waterproofing

Cementitious capillary crystalline waterproofing (CCCW) is the latest type of coating available for reinforcements. This coating is applied onto the reinforcements before pouring concrete. This blocks the entry of migrating corrosion particles. The steel bars can also be coated after placing them in the concrete formwork.

The other advantage of this coating is that the probability of damages caused from handling and transporting are minor because of their self-healing properties, provided they are properly cured. In existing structures, a small layer of CCCW can be applied during rehabilitation of embedded steel reinforcements and around the concrete exposed to weathering (Zhang et al., 2012).

5.2.2. Epoxy-coated rebar

Epoxy-coated rebar resists the entry of chloride and oxygen ions by providing a barricade around the surface area of the embedded steel members. The bars are cleaned thoroughly and coated with epoxy resin in the powdered form. This is then heated and cured at very high temperatures to attain the defined strength. This coating acts like an electrical insulation while minimizing the flow of corrosive current through the members. The major disadvantage of this type of bars is that exceptional care must be taken while handling and storing them, as they can be easily damaged. The bars must also be checked for voids or any other spots that could eventually lead to localized corrosion. The bars are susceptible to corrosion if they are bent as the coating on those bars would tend to peel off easily causing damages (Susca, 2014; Ahmed et al., 2017).

5.2.3. Galvanized rebar

Galvanized rebars are coated with a sacrificial metal such as zinc. Zinc is a noble metal and corrodes slower than steel. Zinc sacrifices itself during the electrochemical reaction which helps in reducing the corrosion in the reinforcing bars. The bars resist corrosion only in the presence of zinc on the bars. Half the world's total production of zinc is mainly for use in the field of corrosion as an anti-corrosive agent (Dallin et al., 2015). It tends to undergo dissimilar metal corrosion if the coated galvanic rebar and uncoated steel comes in contact. Thus, all the metals surrounding the galvanized rebar must also be coated with zinc to avoid corrosion caused due to dissimilar metal corrosion (Susca, 2014; Ogunsanya et al., 2017).

5.2.4. Passive cathodic protection

Passive cathodic protection follows the same principle of galvanized rebar. In the presence of a sacrificial metal, the steel surface undergoes polarization with the help of another more negatively charged potential. This slows the oxidation of steel thereby retarding the formation of corrosion. Most commonly used galvanic anodes are magnesium and aluminum-based alloys as they will continue to sacrifice themselves during electrochemical reactions and will therefore have to be replaced periodically (Cheung et al., 2013).

5.2.5. Water-proof membranes

Water-proof membranes act as a wall defending the ingress of external chlorides into concrete and provide a barricade against the deicing chemicals. This layer blocks the ingress of ions which may lead to corrosion. The waterproof membranes must undergo

the standard tests mentioned in the ASTM D 5385. An ideal waterproofing membrane would have the qualities to withstand changes in weather conditions which induce cracking through expansion and contraction of concrete and the joints. It should also withstand extensive wear caused by constant movement of vehicles and ultra-violet rays (Perkins, 1997; Susca, 2014).

During the application period, blisters or punctures known as blowholes can occur in the membrane. This is caused by expansion of vapors when applied hot. This can be avoided if the membranes are inducted using constant drying during the curing period, provided the atmospheric conditions are suitable for application. After curing, the adhesion of the membrane to the concrete is enough to avoid the formation of blisters. The method of application is often less time consuming when compared to other methods (Perkins, 1997).

5.2.6. Polymer concrete overlays

Polymer concrete overlays have been in use since the 1960s. In this method, a layer of aggregates is affixed to the concrete surface with a polymer binder such as polyesters, acrylics or epoxies. This could be either used directly by spreading over the deck by combining both the aggregates and resin or by premixing and using it with the help of a screed. Polymer concrete undergoes setting quickly and can be produced at the consumer's necessities. Usually, they are placed at a range of ¼ in. to 1½ in. thickness. They have high resistance to abrasion, water and the ingress of chloride ions. They can wear out quickly because of their high shrinkage and thermal expansion coefficients.

Thus, appropriate selection of polymer binders and aggregate gradation is advised (ACI 548.1R, 1997).

Also, they have a low tolerance rate towards moisture and very low temperatures. This requires the substrate to be completely dry and more than 4° C (40° F) higher than the ambient temperature during application. A primary layer or a bond coat of a clean and neat polymer is applied in advance of the application of the polymer concrete. Experimental polymer overlays made from polyester-styrene have recently come into the market and is touted to show better performances than the regular polymer overlays (ACI 548.1R, 1997).

5.2.7. Latex modified concrete overlays

Latex-modified concrete is formed by the addition of polymeric latex to the regular cement concrete. Approximately a 15% replacement of cement with latex is typically used. To avoid coagulation and excessive air entrapment during mixing, the particles are stabilized, antifoaming agents are used to prevent the latter. The cement is well hydrated as there is water dispersion into the latex. Also, this concrete overlay requires low water-cement ratio and provides better durability and resistance against chloride ingress. The most commonly used latex is Styrene-butadiene, but acrylic latexes have also been used (ACI 548.3R, 2003).

The first recorded use of latex-modified overlays dates to 1957, although most of the usage started in the late 1970s. The average thickness used for overlays are between 40 mm and 50 mm (1 ½ in. and 2.0 in.). The latex-modified concrete overlays are usually thinner than the regular low-slump concrete overlays due to high material costs and

superior performance of latex-modified concrete in chloride ingress tests. Due to the latex polymers, air-entraining admixtures are not necessary to provide resistance against freezing and thawing (ACI 548.3R, 2003).

At least an hour before the application, the concrete base must be pre-wet. This is done prior to the process, because the water slows down the film formation of the latex. General wet curing times are between 24 to 72 hours with at least a minimum of 72 hours of dry curing suggested for better results. The concrete develops strengths around a low temperature of about 13℃(55 °F). However, during such temperatures the curing period may be more than 72 hours. Also, the application of the latex-modified concrete overlay is not recommended below a temperature of 7 C (45 F) (ACI 548.3R, 2003).

Most of the properties are like silica fume-modified concrete overlays with decreased bleeding and plastic shrinkage. The entrapment of excessive air also results in problems in the future. This has led to limitation of the air content to 6.5% in most projects. As the air content increases, the flexural and compressive strength of the concrete overlays decreases (ACI 548.3R, 2003).

5.2.8. Silica fume modified concrete overlays

With the help of silica fumes and high range water-reducers, a much lower permeability to chloride ion ingress can be achieved. This type of concrete is considered as superior to that of low-slump concrete when it comes to consolidation and finishing. A water-cement ratio of less than 0.40 can be used leading to lower porosity and permeability (ACI 548.1R, 1997).

The first stage of concrete which comes as slurry or a paste is gently brushed onto the base concrete right before the application of the concrete overlay. Sometimes a stiff-bristle brush is also used to apply a separate bond coat in addition to the mortar. The methods for curing are the same as regular concrete. There is a high possibility of shrinkage cracking as the amount of water used is considerably less which causes low bleeding of concrete. Thus, early curing is required to limit shrinkage cracking (ACI 548.1R, 1997; Perkins, 1997).

Chapter 6. Conclusions and Recommendations

6.1. Summary

Deterioration caused by corrosion is found in many reinforced concrete structures. It may be difficult to investigate the structural elements without disturbing the structural integrity. To overcome this problem, non-destructive tests can be used to evaluate the structure. The results obtained from the GPR, probabilistic corrosion models and structural analyses were found to be satisfactory. Various environmental factors influence corrosion is impossible to arrest the natural forces around the structure. However, various treatment methods are available to slow the onset and progression of corrosion.

6.2. Conclusions

During the investigation, it was observed that the structural drawings lacked vital information about the pre-stressed double T-beams. It was also seen that in certain areas the concrete clear cover did not match the readings obtained from the experiments conducted on-site. This was a setback as it was difficult to perform the analysis. A Profoscope helped in obtaining the depth of concrete clear covers in the present condition. The structural analysis was performed on the prestressed double T-beams, which consists of ½ in. seven-wire strand with Grade-270 and maximum chloride ion content of 0.30. The data secured from the non-destructive testing methods and the probabilistic corrosion models obtained from the deterioration phases reveals the following about the current situation of the parking deck. The on-site experiments conducted using non-destructive methods such as SIR 4000 and Profoscope revealed details about the current condition of the structure. The information obtained from the

experiments also showed that the measurements mentioned in the structural drawings were slightly altered during the construction of the structure.

i. During the analysis of the probabilistic data obtained from the corrosion models, it was observed that for a maximum chloride ion content of 0.30 the residual diameter values of chlorination and carbonation for a ½ in. seven-wire strand were found to be 0.4829 in. and 0.4969 in. The loss of reinforcement area due to chlorination-induced corrosion was estimated to be about 4.24%. This result indicates that most of the corrosion was caused due to chlorination as the loss of reinforcement area due to carbonation is negligible when 0.4969 in. is compared with ½ in. and thus has little or no effect on the structure.

ii. The critical horizontal crack width of corrosion in cracking increased as the concrete clear cover depth increases. When the horizontal length of cracks exceeds the critical values mentioned in Table 4-6, corrosion takes place by depassivation of steel.

iii. From observations, it was established that the presence of cracks on the surface deteriorates the structure. The results obtained for the critical horizontal crack width of concrete clear cover in spalling indicate that surface cracking must be repaired immediately to delay the attack of corrosion on the structure.

6.3. Future works and Recommendations

The service life of the structure can be improved by following the economical remedies mentioned under Section 5.1. Some of the most commonly used measures to prevent

corrosion such as penetrating sealants, passive cathodic protection and latex-modified concrete overlays are easily available. The introduction of these measures will control the ingress of chlorides providing a protective layer against corrosion. The effects of corrosion on reinforced concrete structure are long term. By reviewing the structural drawings and investigating the structure, it is safe to say that both pre-construction and post-construction stages must be given equal importance as chloride ion content, water cement ratio, consolidation, adequate concrete cover depth might help delaying the initiation of corrosion.

The use of reinforced steel has reached an all-time high since its use as a building material. It is time to look for an alternate option which is both economical and eco-friendly. Recently, various research groups have been conducting experiments to produce an environmentally friendly building material. For example, a research facility at ReforceTech, a Norwegian company, developed an innovative material called Basalt Fiber Reinforced polymer (BFRP) Minibars. These minibars have been determined to possess strength-to-weight ratio of about 2.5 times higher than that of alloyed steel which is used as steel reinforcement in construction. These minibars have also satisfied the strength requirements mentioned in ASTM C1609, as recommended by the ACI 318 (2008) for steel fiber reinforced concrete (Brownell, 2015).

The main composition of BFRP minibar is a mixture of polymer resin which binds the bars in a helical shape. The length of these bars varies between 20 mm (0.78 in.) and 200 mm (7.87 in.). The BFRP minibars are mixed directly with the concrete without disrupting the concrete workability. This reduces the need for the use of reinforcement steel. ReforceTech has already started using this technology to manufacture insulated

wall panels. This resulted in a decrease in the thickness from the typical 3 in. to 1½ in. These minibars have a high resistance towards chemicals and thus these minibars might also help in providing corrosion free structures in future. This could also be the answer to the current economic crisis caused by high steel tariffs (Brownell, 2015).

REFERENCES

ACI Committee 222.3R-11. (2011). Guide to Design and Construction Practices to Mitigate Corrosion of Reinforcement in Concrete Structures. Reported by *American Concrete Institute.*

ACI Committee 330R-01. (2001). Guide for Design and Construction of Concrete Parking Lots. Reported by *American Concrete Institute.*

ACI Committee 222R-01. (2001). Protection of Metals in Concrete Against Corrosion. Reported by *American Concrete Institute Committee 222.*

ACI Committee 362. 1R-97. (2002). Guide for the Design of Durable Parking Structures *American Concrete Institute. (Reapproved 2002).*

ACI Committee 309, ACI 309R-05. (2005). Guide for Consolidation of Concrete. *Reported by ACI Committee*.

ACI Committee 548, ACI 548.3R-03. (2003). Polymer-Modified Concrete. *Reported by ACI Committee*.

ACI Committee 548, ACI 548.1R-97. (1997). Guide for the Use of Polymers in Concrete. *Reported by ACI Committee*.

Ahmad, S. (2003). Reinforcement corrosion in concrete structures, its monitoring and service life prediction — a review. *Cement & Concrete Composites 25 459–471. Department of Civil Engineering, King Fahd University of Petroleum and Minerals, 31261 Dhahran, Saudi Arabia.*

Ahmed, I., Manzur, T., & Efaz, I., Mahmood, T. (2017). Experimental Study On Bond Performance of Epoxy Coated Bars And Uncoated Deformed Bars In Concrete. *10.13140/RG.2.2.29563.52004.*

Ann, K. Y., & Song, H. W. (2007). Chloride threshold level for corrosion of steel in concrete, School of Civil and Environmental Engineering, *Yonsei University, Seoul 120-749, Republic of Korea.*

Berkowskia, P., Dmochowskib, G., & Kosior-Kazberukc, M. (2013). Analysis of Structural and Material Degradation of a Car-Park's RC Bearing Structure Due to City Environmental Influences, *Wroclaw University of Technology, Wyb. St. Wyspianskiego 27, PL-50-370 Wroclaw, Poland.*

Bertolini, L., Elsener, B., Pedeferri, P., Redaelli, E., & Polder, R. (2013). Corrosion of Steel in Concrete: Prevention, Diagnosis, Repair, Second Edition. *Wiley-VCH Verlag GmbH & Co. KGaA. Published 2013 by Wiley-VCH Verlag GmbH & Co. KGaA.*

Brownell, B. (2015). "Two Natural Rebar Alternatives for Concrete". www.architectmagazine.com/technology/two-natural-rebar-alternatives-for-concrete_o.

Cheung, M. S., Moe & Cao, Chong. (2013). Application of cathodic protection for controlling macrocell corrosion in chloride contaminated RC structures. *Construction and Building Materials. 45. 199–207. 10.1016/j.conbuildmat.2013.04.010.*

Christodoulou, C., Glass, G., Webb, J., Austin, S., & Goodier, C. Assessing the long term benefits of Impressed Current Cathodic Protection, Corrosion Science, *Volume 52, Issue 8, 2010, Pages 2671-2679, ISSN 0010-938X.*

Cigna, R., Andrade, C., & Nürnberger, U. (2003). COST Action 521, Corrosion of steel in reinforced concrete structures, *Final report. European Communities, Luxembourg*.

Clear, K.C., & Hay, R.E., (1973). "Time-to-Corrosion of Reinforcing Steel in Concrete Slab, V.1: Effect of Mix Design and Construction Parameters," *Report No. FHWA-RD-73-32, Federal Highway Administration, Washington, DC, 103 pages.*

Clear K.C. (1976). "Time-to-Corrosion of Reinforcing Steel in Concrete Slabs," Federal Highway Administration, *PB 258 446, Vol. 3.*

Cody, R. D., Cody, A. M., Spry, P. G., & Gan, G. L. (1996). "Concrete Deterioration by Deicing Salts: An Experimental Study" *Department of Geological and Atmospheric Sciences, 253 Science I, Iowa State University, Ames, Iowa 50011-3210.*

Daczko, J., & Attiogbe, E. (2003). Self-Consolidating Concrete-A Technology for the 21st Century," Structural Engineer. *January 2003*.

Darmawan, M. S., & Stewart, M. G. (2007). Effect of Pitting Corrosion on Capacity of Prestressing Wires, *Magazine of Concrete Research, 59(2), 131-139, 2007.*

Dallin, G., Gagné, M., Goodwin, F., & Pole, S. (2015). Continuously Galvanized Reinforcing Steel.

Dr. Rodriguez, J., Ortega, L. M., & Casal, J. (1997). Load Carrying Capacity of Concrete Structures with Corroded Reinforcement. *Construction and Building Materials, Vol. II, No. 4. pp. 239-248, 1997. Geocisa (Dragados Group), Madrid, Spain. 31 August 1997.*

DuraCrete, Final Technical Report. (2000). General Guidelines for Durability Design and Redesign, *Contract BRPR-CT95-0132, Project BE95-1347 Document BE95-1347/R17, May 2000.*

Farny, J.A. & Kosmatka, S.H. (1997). Diagnosis and Control of Alkali Aggregate Reactions in Concrete, *IS413, Portland Cement Association, 1997, 24 pages.*

Fleming, J. A. (1911). "Electricity". In Chisholm, Hugh. *Encyclopaedia Britannica. **9** (11th ed.). Cambridge University Press. p. 182.*

Fowler, D. W. (1999). Polymers in concrete: a vision for the 21st century, Cement and Concrete Composites, *Volume 21, Issues 5–6, 1999, Pages 449-452, ISSN 0958-9465*.

Geophysical Survey Systems (2016). Inc. SIR 4000 Manual. *40 Simon Street, Nashua, NH 03060-3075. MN72-574 Rev E 18 July 2016.*

Glass, G. K., Page, C. L., & Short, N. R. (1991). Factors Affecting the Corrosion Rate of Steel in Carbonated Mortars. *Department of Civil Engineering, Aston University, Birmingham, U.K, Corrosion Science, Vol. 32, No. 12, pp. 1283-1294, 1991.*

Haavik J. Douglas. (1990). Evaluating concrete cracking by measuring crack width. Consulting Engineer La Habra, *California*. *PUBLICATION #C900553 1990, The Aberdeen Group.*

Hájková, K., Jendele, L., Šmilauer, V., Sajdlová, T., & Červenka, J. (2016). Reinforcement Corrosion in Concrete due to Carbonation and Chloride Ingress up and beyond Induction Period, *Czech Technical University in Prague, Faculty of Civil Engineering Thákurova 7; 166 29, Prague 6; CZ.*

Hansson, C. M., Poursaee, A., & Jaffer, S. J. (2012). Corrosion of Reinforcing Bars in Concrete. *Professor of Materials Engineering, University of Waterloo, Canada, & Ph.D, Candidates, Department of Materials Engineering, University of Waterloo, Canada, December, 2012.*

Hartt, W. H., Powers, R. G., Leroux, V., & Lysogorski, D. K. (2004). Critical Literature Review of High-Performance Corrosion Reinforcements in Concrete Bridge Applications, *Center for Marine Materials Florida Atlantic University—Sea Tech Campus 101 North Beach Road Dania Beach, FL 33004, July 2004.*

Hussain, S. E., Rasheeduzzafar, Al-Mu & am, A., & Al-Gahtani, A. S. (1995). Factors Affecting Threshold Chloride for Reinforcement Corrosion in Concrete. *Royal Commission for Jubail and Yanbu and King Fahd University of Petroleum & Minerals, Dhahran 3 1261, Saudi Arabia, April 19, 1995.*

Jordan, E., & Balmain*, K. G.* (1968). *Electromagnetic Waves and Radiating Systems (2nd ed. Prentice-Hall. p. 100.)*.

Kansas Public Radio, (2009). "Parking Garages: A Multilevel History." November 18, 2009,

Kobrin, G. (1993). "A Practical Manual on Microbiologically Influenced Corrosion", *NACE, Houston, Texas, USA, 1993*.

Koch, G. H., Brongers, P. H., Thompson, N. G., Virmani, Y. P., & Payer, J. H. (2002). "Corrosion costs and preventive strategies in the United States" *FHWA-RD-01-156. Washington, DC: FHWA, March 2002.*

Krauss, P. D., & Naus, D. J. (1998). Repair materials and techniques for concrete structures in nuclear power plants, Nuclear Engineering and Design, *Volume 181, Issues 1–3, 1998, Pages 71-89, ISSN 0029-5493.*

Liu, T., & Weyers, R. W. (1998). Modeling the Dynamic Corrosion Process in Chloride Contaminated Concrete Structures, Cement and Concrete Research, Department of Civil Engineering, *Virginia Polytechnic Institute and State University, Blacksburg, VA 24061 USA, March 1998.*

Melsen, N. V. (2012). "A Short Description of the History of Parking Garages." Friday, December 07, 2012, www.parking-net.com/parking-industry-blog/a-short-description-of-the-history-of-parking-garages.

Millard S, (2003). Measuring the corrosion rate of reinforced concrete using linear polarization resistance. *DTI DME Consortium, Good Practice Guide No 132. Concrete, pp 36-38.*

Millikan, R. A., *& Bishop, E. S.* (1917). Elements of Electricity. *American Technical Society. p. 54.*

Mu, R., Miao, C., Luo, X., & Sun, W. (2002). Cement and Concrete Research 32 (2002) 1061–1066. Interaction between loading, freeze–thaw cycles, and chloride salt attack of concrete with and without steel fiber reinforcement. *Jiangsu Institute of Building Science, No. 12, Beijing Road (w), Nanjing 210008, People's Republic of China, & Department of Materials Science and Engineering, Southeast University, Nanjing 210096, People's Republic of China, January 2002.*

Ogunsanya, I., & Hansson, C. (2017). The Influence of Coating Thickness and Composition on the Corrosion Propagation Rates of Galvanized Rebar in Cracked Concrete. *Corrosion. 74. 10.5006/2370.*

Portland Cement Association (PCA), (2002). Causes of Concrete Deterioration. IS536, Portland *Cement Association, Skokie, Illinois*.

Perkins, P. H. Repair, (1997). Protection and Waterproofing of Concrete Structures, third edition.

Proceq, S. A. (2016). *Operating Instructions–Concrete Test Hammer N. NR–L/LR, Manual, Schwerzenbach, Switzerland.*

Roig-Flores, M., Pirritano, F., Serna, P., & Ferrara, L. (2016). Effect of crystalline admixtures on the self-healing capability of early-age concrete studied by means of permeability and crack closing tests, Construction and Building Materials, *Volume 114, 2016, Pages 447-457, ISSN 0950-0618*.

Šavija, B., & Lukovic, M. (2016). Carbonation of cement paste: Understanding, challenges, and opportunities, Construction and Building Materials *117 (2016) 285–301).*

Susca, S. J. (2014). Treating Reinforcement Corrosion in Parking Structures, Hoffmann Architects, *Volume 31, Number 3, March 2014.*

Taylor, H. F. W. (1997). Cement Chemistry. Published by Thomas Telford Publishing, *1 Heron Quay, London E144JD. 480 pp, £ 65.00. ISBN 0 7277 2592 0, November 1997.*

Teng, L. W., Huang, R., Hsu, H. M., Chen, J., Chao, S. J., & Chen, S. H. (2014). The Research of Concrete Sealer Penetrating Depths, Advanced Materials Research, *Vols. 1025-1026, pp. 703-708, 2014.*

"Vaysburd, A.M., & Emmons. (2000). P.H. Construction and Building Materials 14 _2000. How to make today's repairs durable for tomorrow - corrosion protection in concrete repair. *Structural Preser¨ation Systems, Inc., 3761 Commerce Dri¨e, Suite 414, Baltimore, MD 21227, USA, February 2000.*

Western Specialty Contractors. (2013). "What Are Some Signs of Parking Structure Deteriorations? Avoid Costly Repairs by Maintaining Your Parking Structure, 2013", www.westernspecialtycontractors.com/parking-structure-maintenance/.

Wiwatrojanagul, P., Sahamitmongkol, R., Tangtermsirikul, S., & Khamsemanan, N. (2017). A new method to determine locations of rebars and estimate cover thickness of RC structures using GPR data. *Construction and Building Materials. 140. 257-273.10.1016/j.conbuildmat.2017.02.126.*

Zhang, P., Cong, Y., Vogel, M., Liu, Z., Müller, H. S., Zhu, Y., & Zhao, T. (2017). Steel reinforcement corrosion in concrete under combined actions: The role of freeze-thaw cycles, chloride ingress, and surface impregnation. *Construction and Building Materials 148(2017) 113-121. Center for Durability & Sustainability Studies of Shandong Province, Qingdao University of Technology, Qingdao 266033, PR China, & Institute of Concrete Structures and Building Materials, Karlsruhe Institute of Technology, 76131 Karlsruhe, Germany. 6 May 2017.*

Zhang, R., Castel, A., & François, R. (2010). Concrete cover cracking with reinforcement corrosion of RC beam during chloride-induced corrosion process. Cement and Concrete Research 40 (*2010*) 415–425. *Modern Design and Analysis Research Institute, Northeastern University, Shenyang, China. LMDC (Laboratoire Matériaux et Durabilité des Constructions), Université de Toulouse, UPS, INSA, Toulouse, France. Accepted 29 September 2009.*

Zhang, Y., Li Du, X., Li, Y., Min Yang, F., & Zhan, G. L. (2012). Research on Cementitious Capillary Crystalline Waterproofing Coating for Underground Concrete Works. *Advanced Materials Research. 450-451. 286-290. 10.4028/scientific5/AMR.450-451.286.*

Zhu, F., Ma Z., & Zhao, T. (2016). Influence of Freeze-Thaw Damage on the Steel Corrosion and Bond-Slip Behavior in the Reinforced Concrete. *School of Civil Engineering and Architecture, Suqian College, Suqian 223800, China, & Department of Structural Engineering, Tongji University, Siping Road, Shanghai 200092, China, & College of Civil Engineering, Qingdao University of Technology, Fushun Road, Qingdao 266033, China. Accepted 11 July 2016.*

APPENDICES

Appendix A. Structural drawings of Lincoln Parking Deck provided by FMS at YSU

1. Level 1 Plan

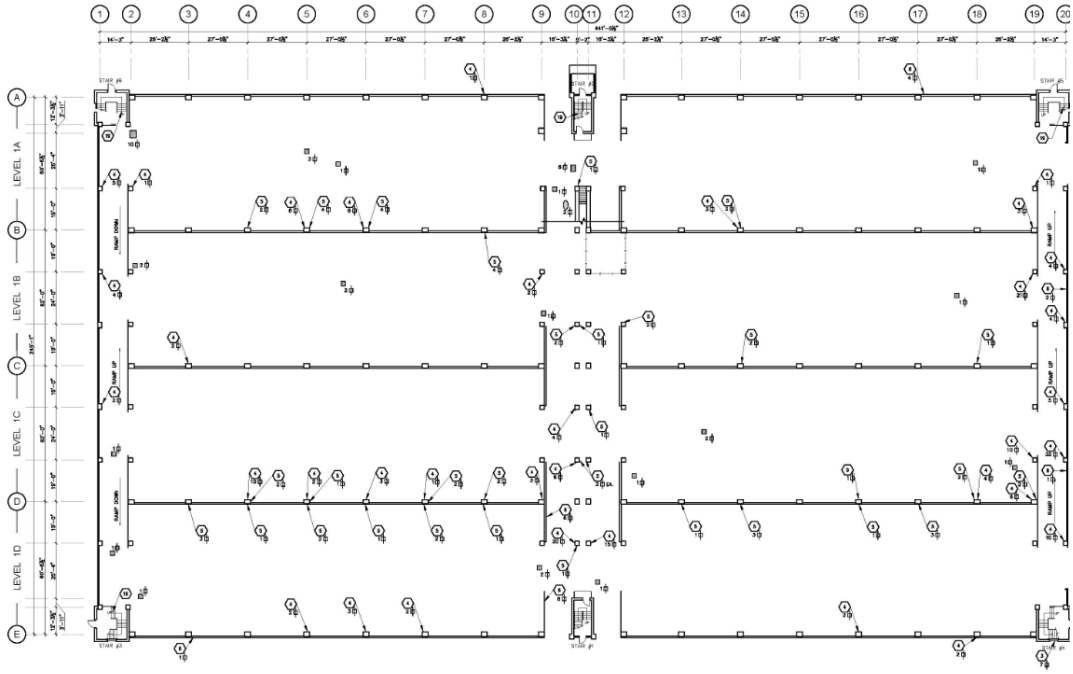

2. Level 2 Plan

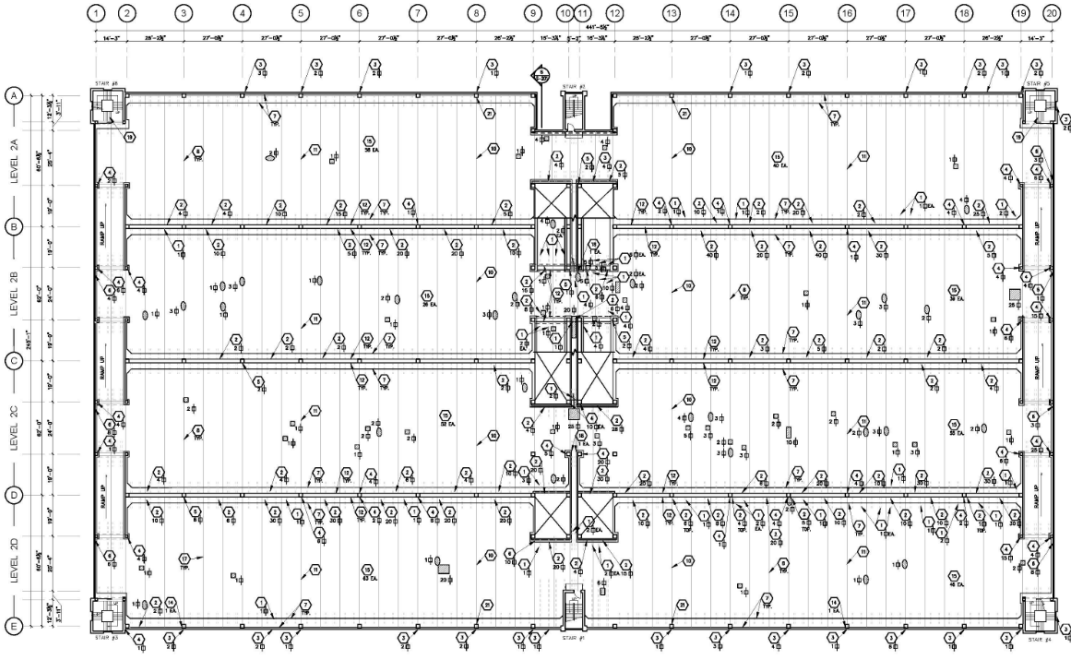

3. Level 3 Plan

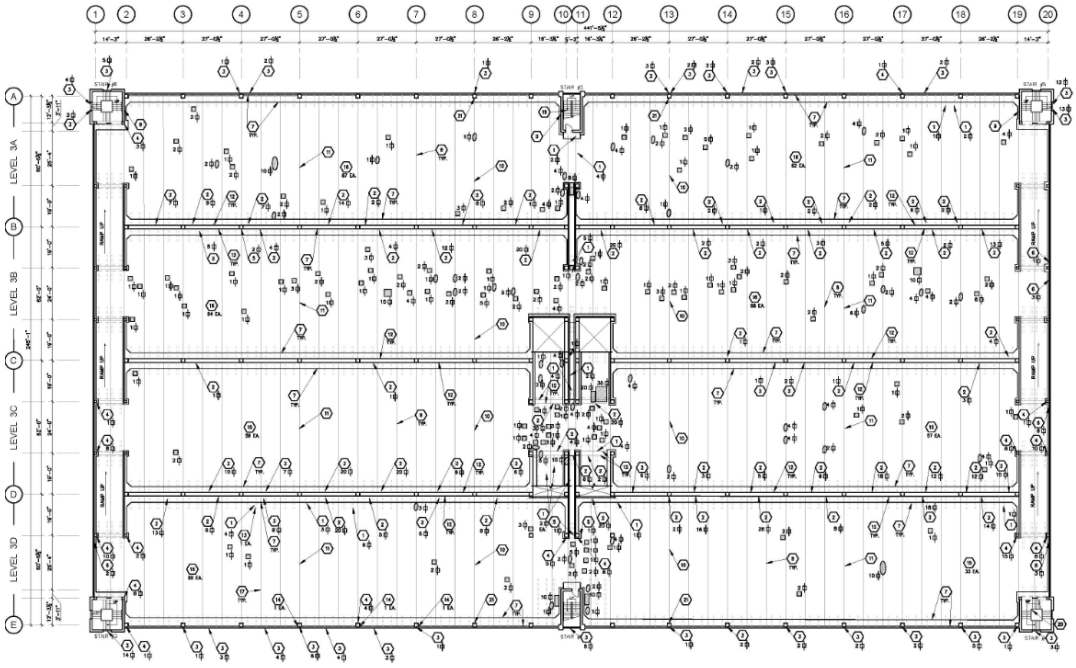

4. Level 4 Plan

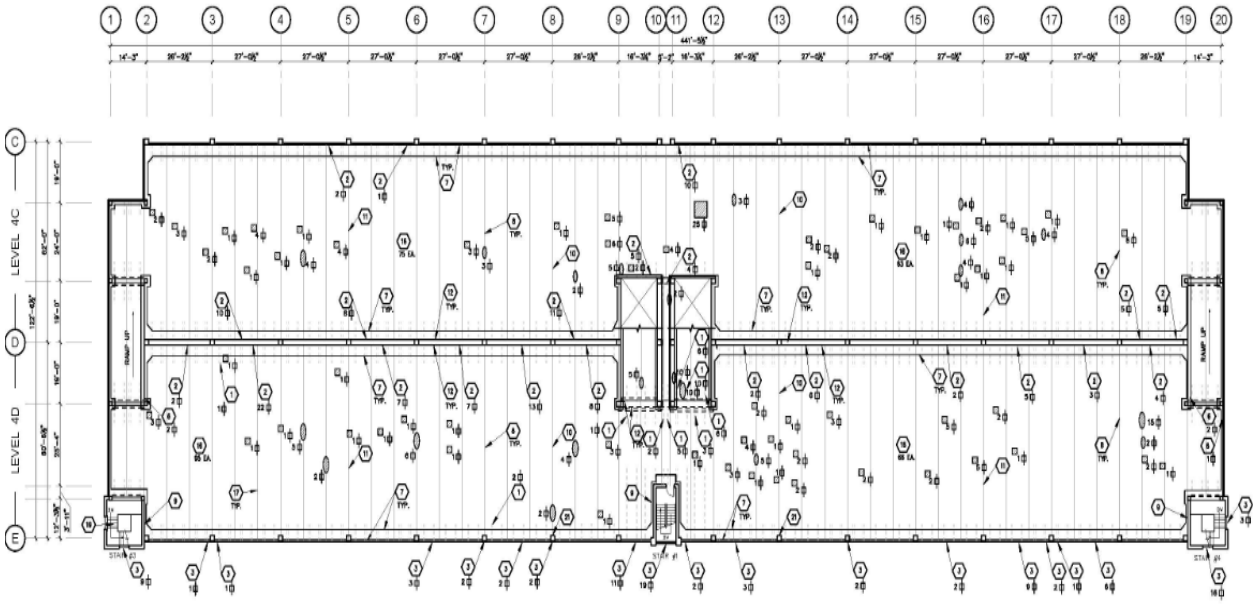

Appendix B. Average diameter and standard deviation of rebars

	Section														
	1	2	3	4	5	6	7	8	9	10	11	12	13	14	15
Dia (in)	0.5	0.5	0.5	0.5	0.5	0.5	0.5	0.5	0.5	0.5	0.5	0.5	0.5	0.5	0.5
	0.49	0.5	0.5	0.49	0.49	0.5	0.48	0.49	0.5	0.5	0.49	0.49	0.5	0.49	0.5
	0.49	0.5	0.5	0.48	0.49	0.5	0.48	0.48	0.5	0.5	0.48	0.48	0.5	0.49	0.5
	0.5	0.5	0.5	0.5	0.5	0.5	0.5	0.5	0.5	0.5	0.5	0.5	0.5	0.5	0.5
	0.5	0.5	0.5	0.5	0.5	0.5	0.5	0.5	0.5	0.5	0.5	0.5	0.5	0.5	0.5
Avg. Dia. (in)	0.496	0.5	0.5	0.494	0.496	0.5	0.492	0.494	0.5	0.5	0.494	0.494	0.5	0.5	0.5
Std. Dev.	0.005	0	0	0.009	0.005	0	0.01	0.0089	0	0	0.0089	0.009	0	0.01	0

Appendix C. Calculation of moment capacity and stresses in concrete and steel

Concrete Strength (fc') = 5 ksi

Yielding Stress of low-relaxation seven wire strand (f_{pu}) = 270 ksi

1. Initial Condition

a. Calculation of flexural strength of prestressed member

$A_s = 14 \times 0.153 = 2.142$ in^2

$f_{pu} = 270$ ksi

$$\rho_p = \frac{A_{ps}}{bd_p} = \frac{2.142}{(48 \times 34) - 2(21.5 \times 30)} = 0.00626$$

For low-relaxation stand, $\frac{f_{py}}{f_{pu}} = 0.90$, $\gamma_p = 0.28$

Therefore, the flexural strength of prestressed member is,

$$f_{ps} = f_{pu}\left[1 - \frac{\gamma_p}{\beta_I}\ \rho_p\ \frac{f_{pu}}{f_c'}\right]$$

$$= 270\left[1 - \frac{0.28}{0.80} \times 0.00626 \times \frac{270}{5}\right]$$

$f_{ps} = 238.055$ ksi

b. Calculation of moment capacity:

$$a = \frac{A_{ps} f_{ps}}{0.85 f_c' b_f} = \frac{2.142 \times 238.055}{0.85 \times 5 \times 48} = 2.50"$$

$$c = \frac{a}{\beta_I} = \frac{2.5}{0.80} = 3.125"$$

Check for tension controlled section

$$\epsilon_t = \frac{d - c}{c} \times 0.003 \geq 0.005$$

$$= \frac{30.04 - 3.125}{3.125} \times 0.003$$

$= 0.025 > \epsilon_t = 0.005$

So, the section is tension controlled, $\varphi = 0.9$

OK.

Therefore, the nominal moment strength of the section is,

$$\varphi M_n = \varphi A_{ps} f_{ps} (d_p - \frac{a}{2})$$

$$= 0.9 \times [2.142 \times 238.055 (30.04 - \frac{2.50}{2})] \times \frac{1}{12}$$

$$\varphi M_n = 1101.032 \text{ k-ft}$$

c. Calculation of Stresses:

$$\text{Modular ratio } (\eta) = \frac{E_s}{E_c} = \frac{29000 \times 1000}{57000\sqrt{5000}} = 7.19 \approx 7$$

Location of neutral axis (NA)

Assume NA is in the web,

$$(b_f - b_w) b_f (y - \frac{h_f}{2}) + \frac{b_w y^2}{2} = \eta A_s (d - y)$$

$$(48 - 5)\, 4\, (y - \frac{4}{2}) + \frac{(5 \times y^2)}{2} = 7 \times 2.142(30.04 - y)$$

Therefore, neutral axis depth, $y = 4.03$"

Assumption is true, Neutral Axis is in the web.

OK

d. Cracking moment of inertia

$$I_{cr} = (\frac{b_f - b_w}{12}) h_f^3 + (b_f - b_w) h_f (y - \frac{h_f}{2})^2 + \frac{b_w y^3}{12} + b_w y(\frac{y}{2}) + n A_s (d - y)^2$$

$$I_{cr} = \frac{(48 - 5)}{12} \times 4^3 + (48 - 5)\, 4\, (4.03 - \frac{4}{2})^2 + \frac{5 \times 4.03^3}{12} +$$

$$\frac{\left(5 \times 4.03^2\right)}{2} + 7 \times 2.142\ (30.04 - 4.03)^2$$

$I_{cr} = 11149.71\ in^4$

i. Compressive stress in steel

$$f_s = \frac{\eta \times M \times (d - y)}{I_{cr}} = \frac{12 \times 7 \times 1101.032 \times (30.04 - 4.03)}{11149.71}$$

$= 215.75\ ksi < f_{pu} = 270\ ksi$

OK

ii. Compressive stress in concrete

$$f_c = \frac{M_y}{I_{cr}} = \frac{1101.032 \times 4.03 \times 12}{11149.71}$$

$f_c = 4.77\ ksi < f_c' = 5\ ksi$

OK

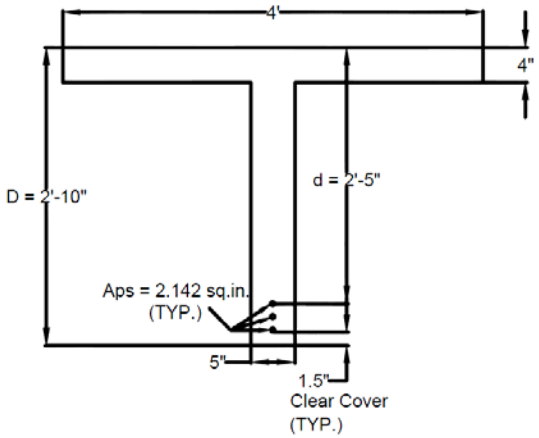

ORIGINAL T BEAM SECTION (N.T.S)

2. Current Condition (with 4.24% loss in reinforcement area)

a. Calculation of flexural strength of prestressed member

$A_s = 14 \times 0.1465 = 2.051 \text{ in}^2$

$f_{pu} = 270$ ksi

$$\rho_p = \frac{A_{ps}}{bd_p} = \frac{2.051}{(48 \times 34) - 2(21.5 \times 30)} = 0.00599$$

For low-relaxation stand, $\frac{f_{py}}{f_{pu}} = 0.90$, $\gamma_p = 0.28$

Therefore, the flexural strength of prestressed member is,

$$f_{ps} = f_{pu}\left[1 - \frac{\gamma_p}{\beta_I}\ \rho_p\ \frac{f_{pu}}{f_c'}\right]$$

$$= 270\left[1 - \frac{0.28}{0.80} \times 0.00599 \times \frac{270}{5}\right]$$

$f_{ps} = 239.433$ ksi

b. Calculation of moment capacity:

$$a = \frac{A_{ps} f_{ps}}{0.85 f_c' b_f} = \frac{2.051 \times 239.433}{0.85 \times 5 \times 48} = 2.40"$$

$$c = \frac{a}{\beta_I} = \frac{2.40}{0.80} = 3"$$

Check for tension controlled section.

$$\epsilon_t = \frac{d-c}{c} \times 0.003 \geq 0.005$$

$$= \frac{30.89-3}{3} \times 0.003$$

$= 0.02789 > \epsilon_t = 0.005$

So, the section is tension controlled, $\varphi = 0.9$

OK

Therefore, the nominal moment strength of the section is,

$\varphi M_n = \varphi A_{ps} f_{ps} (d_p - \frac{a}{2})$

$= 0.9 \times [2.051 \times 239.433 (30.89 - \frac{3}{2})] \times \frac{1}{12}$

$\varphi M_n = 1093.50$ k-ft

c. Calculation of Stresses:

Modular ratio $(\eta) = \frac{E_s}{E_c} = \frac{29000 \times 1000}{57000\sqrt{5000}} = 7.19 \approx 7$

Location of neutral axis (NA)

Assume NA is in the web,

$(b_f - b_w) b_f (y - \frac{h_f}{2}) + \frac{b_w y^2}{2} = \eta A_s (d - y)$

$(48 - 5)\ 4\ (y - \frac{4}{2}) + \frac{(5 \times y^2)}{2} = 7 \times 2.051(30.89 - y)$

Therefore, neutral axis depth, $y = 4.01$"

Assumption is true; Neutral Axis is in the web.

OK

d. Cracking moment of inertia

$I_{cr} = (\frac{b_f - b_w}{12}) h_f^3 + (b_f - b_w) h_f (y - \frac{h_f}{2})^2 + \frac{b_w y^3}{12} + b_w y(\frac{y}{2}) + n A_s(d - y)^2$

$I_{cr} = \frac{(48 - 5)}{12} \times 4^3 + (48 - 5)\ 4\ (4.01 - \frac{4}{2})^2 + \frac{5 \times 4.01^3}{12} +$

$\frac{(5 \times 4.03^2)}{2} + 7 \times 2.051\ (30.89 - 4.01)^2$

$I_{cr} = 11364.71358$ in^4

iii. Compressive stress in steel

$$f_s = \frac{\eta \times M \times (d - y)}{I_{cr}} = \frac{12 \times 7 \times 1093.50 \times (30.89 - 4.01)}{11364.71358}$$

$= 217.25 \text{ ksi} < f_{pu} = 270 \text{ ksi}$

OK

iv. Compressive stress in concrete

$$f_c = \frac{M_y}{I_{cr}} = \frac{1093.50 \times 4.01 \times 12}{11364.71358}$$

$f_c = 4.63 \text{ ksi} < f_c' = 5 \text{ ksi}$

OK

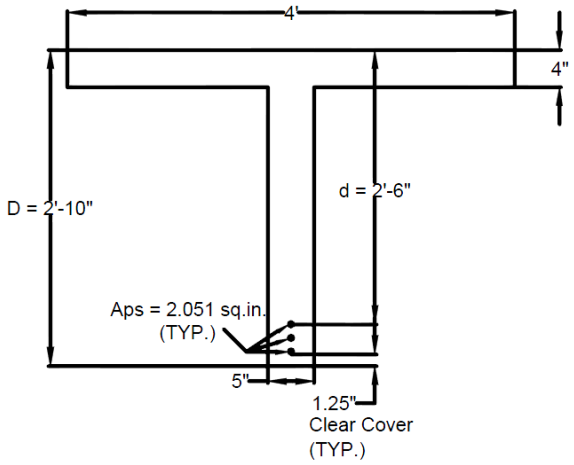

CURRENT T BEAM SECTION
(N.T.S)